JOURNAL OF GEOPHYSICAL RESEARCH, VOL. 86, NO. A6, PAGES 4649-4670, JUNE 1, 1981

NONDUCTED COHERENT VLF WAVES AND ASSOCIATED TRIGGERED EMISSIONS OBSERVED ON THE ISEE-1 SATELLITE

T. F. Bell, U. S. Inan, and R. A. Helliwell

Radioscience Laboratory, Stanford University, Stanford, California 94305

Abstract. The ISEE-1 spacecraft has been an important component of VLF wave injection experiments for studying interactions between coherent VLF waves and energetic particles. The coherent waves are injected into the magnetosphere by ground-based transmitters such as that at Siple Station, Antarctica (76°W, 84°S geographic, L ~ 4.1), and those of the worldwide Omega navigation network. During the period October 1977-August 1979, the Stanford VLF receiver on ISEE-1 acquired data on approximately 90 separate orbits in the plasmasphere in which the satellite longitude lay within 30° of the magnetic field lines linking the North Dakota Omega transmitter (98°W, 46°N geographic, L ~ 3.5). During 12 passes the nonducted Omega signals at 10.2 kHz were observed to trigger VLF emissions on magnetic shells ranging from L = 1.8-3.8. The emission characteristics often differed significantly from those of emissions triggered by ducted signals and detected at ground stations. In many cases each of the triggered signals consisted of a large array of discrete rising tones whose rate of change of frequency approached 40 kHz/sec, a value much larger than that usually associated with emissions triggered by ducted signals. The emission activity occurred during periods in which signals propagated to the spacecraft on at least two separate ray paths of disparate time delay and with a received signal duration of 2 to 4 times that of the transmitted pulses. Typically, the emission activity took place only along the paths of longer time delay. Unusual emission activity involving signals from the Siple Station transmitter was also observed on two occasions outside the plasmasphere. Our results indicate that the emission generation process can take place under much more general conditions that previously believed.

Introduction

This paper reports new observations of nonducted coherent VLF waves from ground-based transmitters and associated VLF emissions in the magnetosphere. The data reported were acquired by the Stanford University VLF Wave Injection Experiment on the ISEE-1 satellite[Bell and Helliwell, 1978]. The experiment has four main components: (1) a broadband (1-32 kHz) VLF receiver on ISEE-1 connected to a long electric antenna, (2) a broadband (1-20)kHz controllable VLF transmitter located at Siple Station, Antarctica [Helliwell and Katsufrakis, 1974], (3) various VLF navigation and communications transmitters, such as those of the worldwide Omega network, and (4) ground stations in the Antarctic and Canada. The main goal of this experiment is to acquire understanding of interactions between coherent VLF waves and energetic particles in the magnetosphere, in particular the whistler mode instability through which both natural and stimulated VLF emissions are produced. Sources of the coherent VLF waves involved in these studies include VLF transmitters, large-scale power grids, whistlers, and other natural coherent VLF signals. The Stanford University experiment on ISEE-1 is an outgrowth of classic 'ground-to-ground' VLF wave injection experiments carried out over the past 5 years using the Stanford University broadband transmitter at Siple Station [Helliwell and Katsufrakis, 1974]. However, there are a number of important differences between the ground-to-ground experiments and the 'ground-to-satellite' experiments described in the present paper.

As shown in the sketch of Figure 1a, in a typical mode of operation of the ground-to-ground experiments VLF waves are injected into the ionosphere from a ground-based source, such as a VLF transmitter, and a small fraction of these waves travel in ducts of enhanced ionization along paths that are closely aligned with the earth's magnetic field. Near the magnetic equatorial plane these waves interact with energetic electrons to produce wave amplification (up to 30 dB), triggering of VLF emissions, and scattering of energetic electrons in pitch angle and energy [Helliwell and Katsufrakis, 1974; McPherson et al., 1974; Dowden et al., 1978].

The injected signals and the associated triggered emissions travel to the ionospheric region conjugate to the source and can enter the earth-ionosphere waveguide to be observed on the ground. An example of such a triggered emission is shown in the lower panel of Figure 1a. On the other end of the field line the scattered electrons precipitate into the ionosphere causing a variety of perturbations that can be detected from the ground. For example, fluxes of natural VLF wave-induced precipitation have been observed to excite X rays [Rosenberg et al., 1971], photoemissions [Helliwell et al., 1980a], and electron density enhancements [Helliwell et al., 1973].

Although ground-based experiments can determine a number of important features of the interaction, *in situ* satellite measurements are required to determine the wave and particle properties in or close to the interaction region. In addition, such measurements represent the only means of studying the class of injected waves which are nonducted. In general, most of the waves injected by a ground-based transmitter propagate in the magnetosphere in a nonducted mode. Although these waves are capable of strong interaction with energetic particles in the magnetosphere, the

Paper number 80A1347.
0148-0227/81/080A-1347$01.00

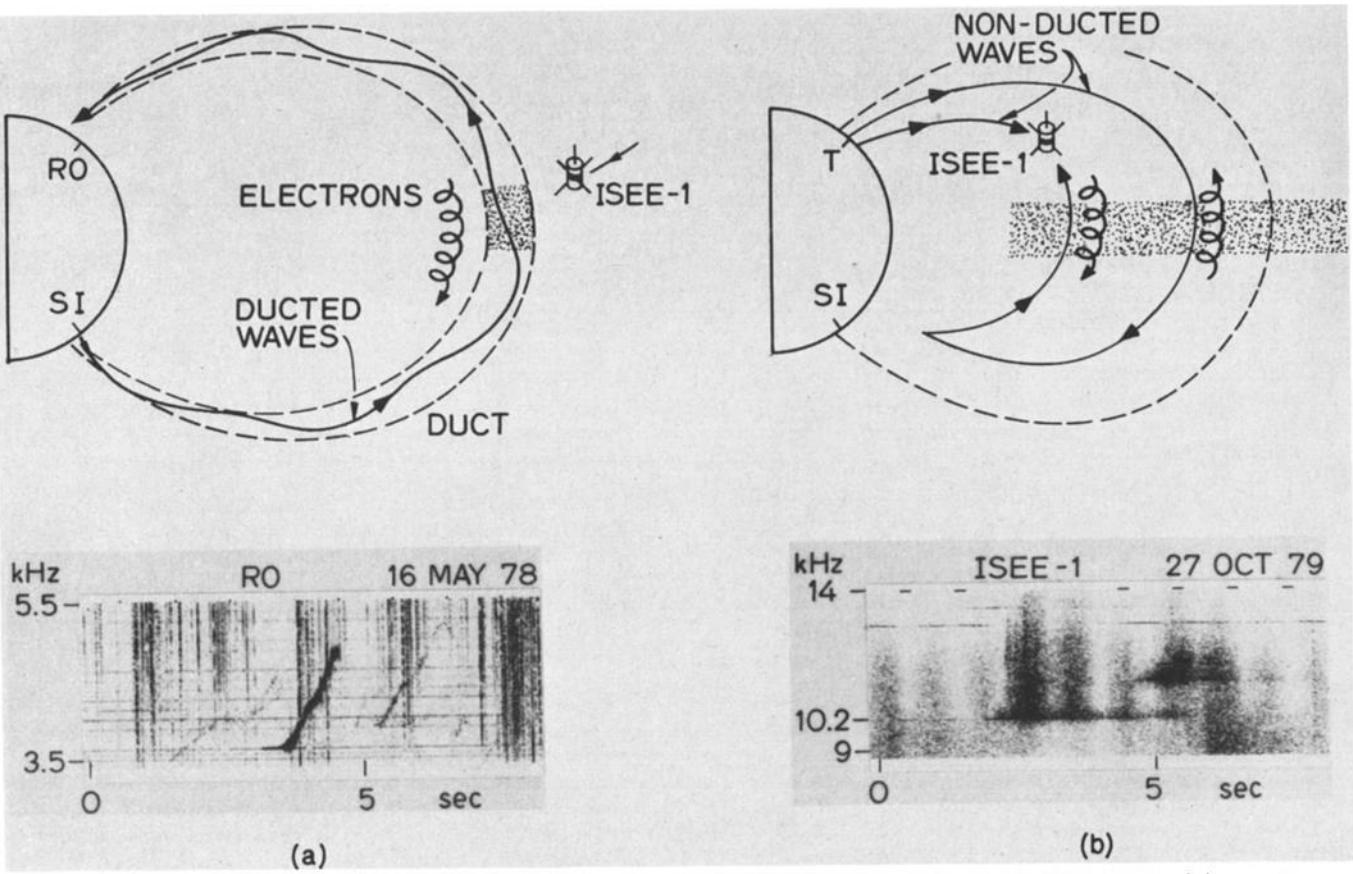

Fig. 1. Schematic representation of two classes of wave-injection experiments. (a) The classic case of ground-to-ground experimentation in which both the source and observation points are ground-based. In these experiments a small fraction of the total injected wave energy travels in ducts of enhanced ionization along paths that are closely aligned with the earth's magnetic field. In the interaction region (shaded) near the magnetic equatorial plane these waves interact with energetic electrons (solid arrow) to produce wave amplification, triggering of VLF emissions and scattering of energetic electrons. The injected signals and associated emissions then propagate in the duct to the ionospheric region approximately conjugate to the source, enter the earth-ionosphere waveguide, and are observed on the ground. A spectrogram of a typical emission triggered by a ducted wave in this type of experiment is shown in the lower portion. In this example recorded at Roberval, the ground station conjugate to Siple Station, a 1-s-long pulse from the Siple Station transmitter at 3.6 kHz triggers a strong VLF emission which rises in frequency for approximately 1 s at a rate of approximately 2 kHz/s. (b) The case of ground-to-satellite experimentation in which the main observation point is satellite-based. This is the case considered in the present paper. In these experiments the injected waves generally travel in a nonducted mode with high wave normal angle and can reach the satellite through a number of distinct ray paths. Nonducted waves can be divided into two groups, the direct waves which reach the satellite directly, and the indirect waves, or echoes, which reach the satellite only after undergoing one or more reflections. Both classes of waves can intersect the interaction region (shown shaded), where they can interact with energetic electrons (solid arrows) to produce wave amplification, triggering of VLF emissions, and scattering of energetic particles. A spectrogram of a typical emission triggered by a nonducted wave in this type of experiment is shown in the lower portion. In this example, observed on the ISEE-1 satellite, pulses from the North Dakota Omega transmitter at 10.2 and 11 1/3 kHz, with durations of 1.2 and 0.9 s respectively, trigger bursts of VLF emissions while propagating to the satellite via an indirect path. The individual elements of each emission burst rise in frequency at a rate approaching 40 kHz/s.

output of these interactions is not observable on the ground because the nonducted waves generally cannot penetrate the lower ionosphere. Thus the only means of observing the output of wave-particle interactions involving nonducted injected waves is through the use of satellites. It is the ground-to-satellite injection experiments which are the subject of the present paper.

As shown in Figure 1b, the nonducted waves propagate in the magnetosphere along non-field-aligned paths, usually with high wave normal

angles. Such waves reach the satellite along 'direct' ray paths, which involve no reflections, or along indirect paths of longer time delay which involve either magnetospheric reflection [Walter and Angerami, 1969] or a specular reflection at the lower ionosphere. For simplicity, the figure shows only one reflected wave component. However, in experimental situations such as our own, waves can arrive at the satellite after experiencing large numbers of reflections in both hemispheres [Edgar, 1976]. The case of multiple reflections of waves is discussed in the appendix. Although the nonducted waves are not confined to a particular field line, they can be expected to interact with energetic particles during each traversal through the interaction region, thought to lie near the magnetic equatorial plane. During some of these traversals the nonducted waves can be expected to trigger VLF emissions. A typical example of one such emission is shown in the lower portion of Figure 1b. As shown in the following sections, the characteristics of emissions triggered by the nonducted waves differ in a number of important respects from emissions triggered by ducted waves.

During these wave injection experiments the Stanford ISEE-1 VLF receiver determines the properties of the interactive waves within, or near, the interaction region. The energetic particle properties are in turn measured by particle experiments also on ISEE-1. Correlation of these measurements then helps to provide a description of the physics of the nonlinear whistler mode instability which produces the wave amplification, the emission generation, and the particle scattering effects.

In the present paper we describe only the wave phenomena observed on ISEE-1 during the wave injection experiments. Description of the concurrent wave-particle correlations will be presented in a future paper.

During the first 2 years of spacecraft operation the two main sources of coherent waves for the Stanford experiment have been (1) the VLF transmitter at Siple Station, Antarctica, with its precisely controlled frequency and amplitude characteristics and (2) the Omega VLF navigational transmitter located in North Dakota. With the aid of these sources the Stanford experiment has acquired data concerning the characteristics of nonducted coherent waves and associated triggered VLF emissions in the magnetosphere.

In this paper we present examples of nonducted coherent VLF signals from the Siple and North Dakota Omega transmitters detected by ISEE-1 over large regions of the plasmasphere and show that the associated triggered emissions differ in several important respects from those associated with ducted waves.

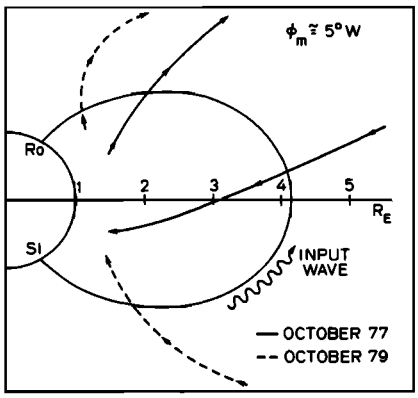

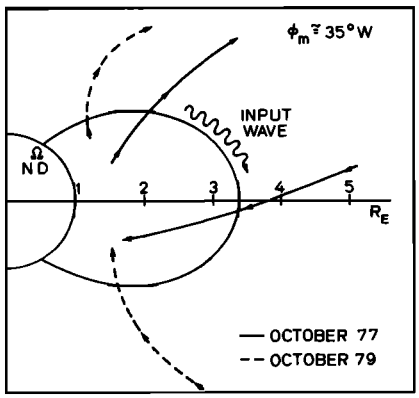

Fig. 2. ISEE-1 inbound and outbound orbits. (a) Projected on the Siple-Roberval meridional plane. (b) Projected on the meridional plane intersecting the location of the Omega transmitter in North Dakota. Orbit configurations shortly after launch (October 1977) and approximately 2 years after launch (October 1979) are both shown.

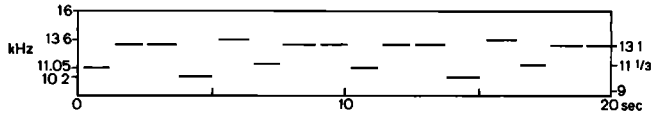

Fig. 3. North Dakota Omega transmission format for 10.2, 11.05, 11 1/3, 13.1, and 13.6 kHz. Pulse lengths vary from 0.9 to 1.2 s. The pulse length for the 10.2-kHz pulses is 1.2 s. The format is repeated every 10 s.

Experiment Background

Figure 2 depicts the inbound and the outbound legs of typical ISEE-1 orbits near the longitude of the Siple-Roberval magnetic meridian (magnetic longitude, ϕ_m, ~5°W) and the longitude of the North Dakota Omega magnetic meridian (ϕ_m ~35°W). Inbound and outbound legs are shown for two time periods, October 1977 (launch) and October 1979. In each case the orbits have been projected onto the appropriate meridional plane.

Siple and Roberval stations are magnetically conjugate and lie at the base of the L ~ 4.1 magnetic shell. The North Dakota Omega transmitter lies at the base of the L ~ 3.5 magnetic shell.

As shown in Figure 2a, measurements of Siple signals near or within the interaction region (magnetic equator) in the range $2 \leq L \leq 4$ were possible on the inbound leg of the ISEE-1 orbit for a few months immediately following launch on October 1977. The inclination of the ISEE-1 orbit at that time was approximately 30°, but

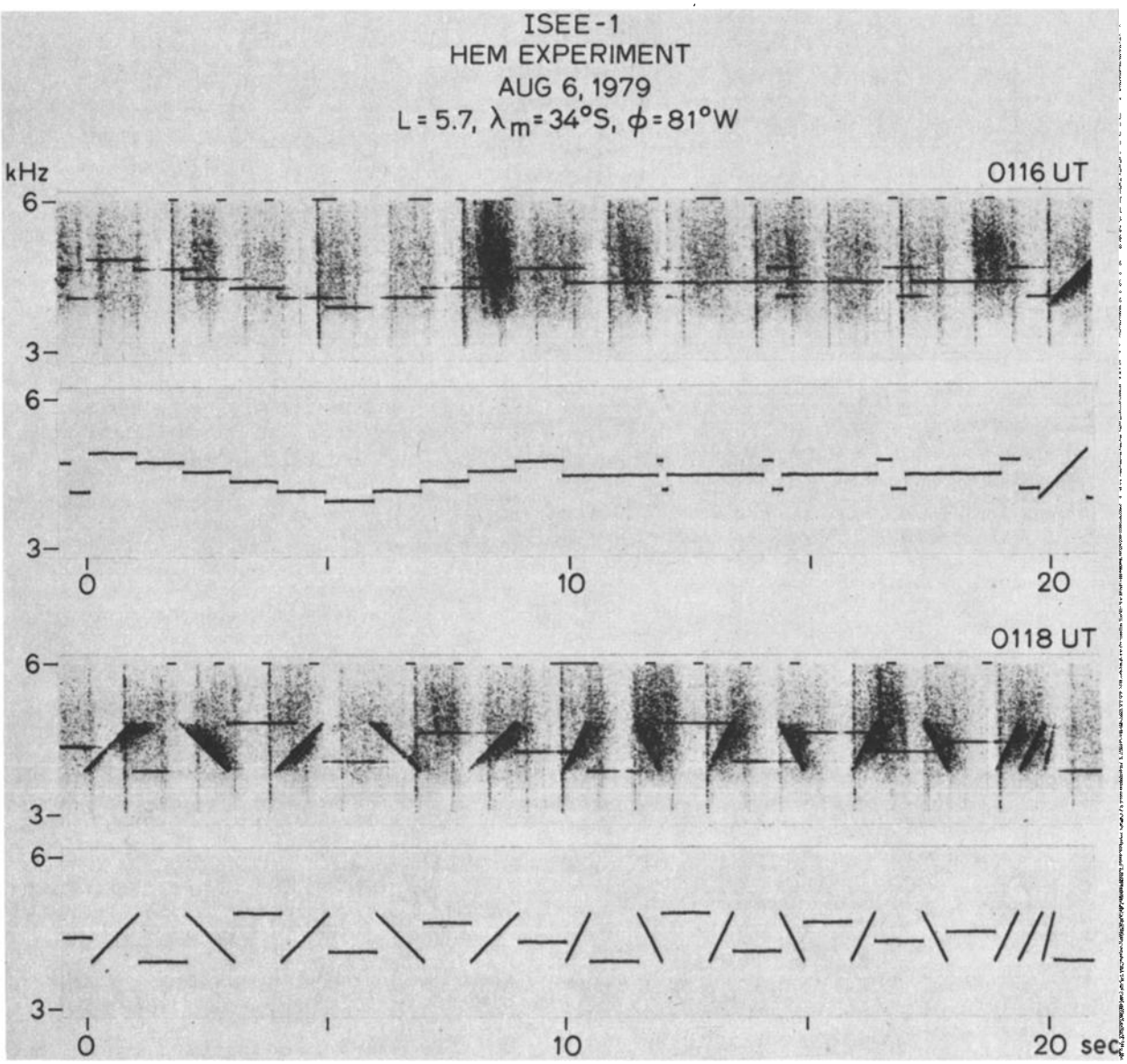

Fig. 4. Examples of transmission formats employed by the Siple transmitter and typical examples of these signals as received on the ISEE-1 satellite.

by October 1979 the inclination had increased to 52° and the inbound leg lay far to the south of the interaction region, generally allowing measurement of the signals only prior to their traversal of the interaction region and thus prior to the times of emission triggering.

On the other hand, the outbound legs of the orbit during the 2-year period provided data only on the output waves from the interaction region. The general character of these orbits was not a function of the inclination angle. As a consequence, the data on VLF emissions triggered by nonducted Siple signals have been obtained largely on the outbound leg of the ISEE orbit.

Measurements of Omega signals were made in the $2 \leq L \leq 4$ range within and slightly to the south of the interaction region on the inbound leg of the ISEE-1 orbit, as shown in Figure 2b. Thus on the inbound leg, the output waves from the interaction region could be readily measured. This situation had not changed radically by October 1979.

Omega data acquired on the outbound leg of the orbit were limited mainly to direct input waves, that is, those that had not crossed the equator. However, occasionally, Omega signals were observed both in the direct mode and also in a reflected mode after having been reflected at the ionosphere in the southern hemisphere. This mode of propagation is shown in Figure 1b. In some cases, these 'echoes' were accompanied by VLF emissions which had presumably been triggered by the direct input signals as they passed through the interaction region. Thus data acquired on the outbound leg near the North Dakota Omega meridian included both the wave input to the interaction region and the wave output from this region.

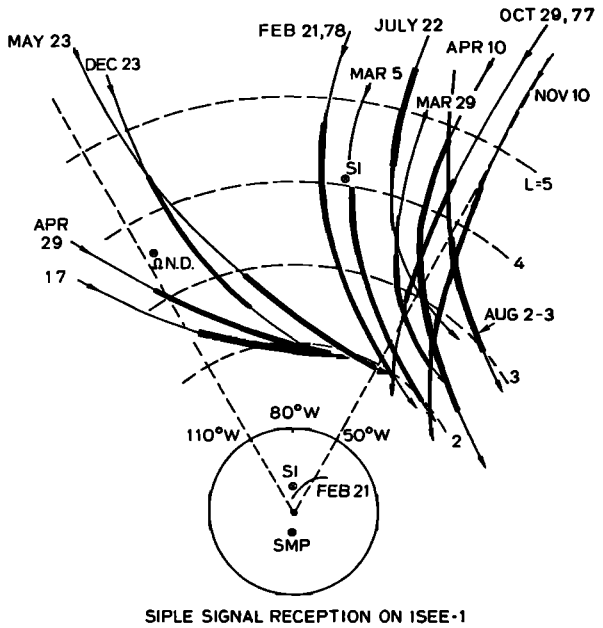

Fig. 5. Viewing area of the Siple transmitter, mapped onto the geomagnetic equatorial plane in a centered dipole system. The angular scale gives geographic longitude. Portions of the ISEE-1 orbits for the period October 29, 1977, to August 2, 1978, are shown. The heavy lines indicate the times when the transmitter signals were received on the satellite. The intersection with the equatorial plane of the magnetic field lines through the Siple and Omega transmitters are indicated by circled crosses. Points of reception of signals from the North Dakota Omega transmitter are not shown, but these signals were observed on nearly all of the portions of the orbits shown that lay in the range $1.5 < L < 4$ (see Figure 8).

Partially as a result of these orbital considerations the observed incidence of VLF emission triggering on ISEE-1 was approximately 3 times as high for Omega signals as it was for Siple signals. Other factors contributing to this disparity include differences in transmitter output power (Siple ~ 1 kW at 6 kHz; Omega ~ 10 kW), location, and operation frequency.

Because of the navigational mission of the Omega transmitter only the standard modulation format was available for observation by the ISEE-1 satellite. This format, shown in Figure 3, consists of continuously repeated segments of 10-s duration. Each segment has eight fixed-frequency pulses of fixed duration at 10.2 (one pulse), 11.05 (one pulse), 11 1/3 (one pulse), 13.1 (four pulses), and 13.6 kHz (one pulse). Each pulse is separated in time from its successor by 200 ms, and the average pulse length is approximately 1 s.

During the ISEE-1 wave injection experiments from Siple Station, several transmission formats were used, examples of which are shown in Figure 4. In general, the formats are a series of fixed-frequency pulses of variable duration as well as variable frequency ramps of both positive and negative slope. Each format is designed to investigate one or more specific questions concerning the physics of the wave-particle interaction which leads to the triggering of VLF emissions. For example, the variable pulse length format shown in the upper panel of Figure 4 was designed to study the effect of input pulse length on the emission process [Stiles and Helliwell, 1975] and to determine on which side of the earth's magnetic equator the generation of rising and falling tones takes place [Helliwell, 1967]. The 'stair-step' format, also shown in the upper panel, is designed to study the dependence of the emission process on input wave frequency and to study the wave entrainment process [Helliwell and Katsufrakis, 1974] in which triggered emissions are 'captured' or entrained by subsequent transmitter pulses. Finally, the ramp format of the lower panel is designed to study multipath effects and the effect upon the emission process of changes in the frequency of the input wave and to determine how the wave growth rate varies with the sign and magnitude of df/dt. In general, the output power varies by less than 3 dB throughout each ramp with the maximum output produced at the center frequency. In all formats the input wave amplitude can also be varied to show how emission generation depends on wave amplitude. Typical examples of these formats as received on the satellite are shown above each panel. Note that the received pulses are longer than the transmitted ones. This pulse elongation is produced whenever multiple paths of propagation of disparate group time delay exist between the ground and the satellite. This effect is also evident in the receptions of the frequency ramp format (lower panel), where each discrete ramp of minimum time delay is seen to be followed by a diffuse distribution of a number of ramps that reach the satellite at different times (see the appendix).

In the following sections we first present data on the distribution of coherent nonducted waves in the magnetosphere and then report on the new observations of triggering of VLF emissions by these waves. Interpretation of the data presented requires that the magnetospheric ray path(s) from the transmitter to the satellite be identified and that the wave characteristics along this path be determined. In most of the data there was clear evidence that the observed signals propagated to the satellite along non-field-aligned (i.e., nonducted)paths, with time delays of ~1 to ~4 s. As a result of the superposition of the signals from these different paths, the observed pulse duration greatly exceeded that of the transmitted pulse (~1-1.2 s). The magnetospheric ray paths can be determined by reconciling the time delay and multipath properties of the received signals with the results of raytracing studies in a model magnetosphere.

Typical ray paths of 10.2-kHz (Omega) and 5-kHz (Siple) signals in the inner magnetosphere are discussed in the appendix for a simple magnetospheric model. The results show that in general there are two kinds of signals that reach the satellite: (1) the direct pulse arriving at the satellite prior to any reflections, and (2) the echoes that arrive at

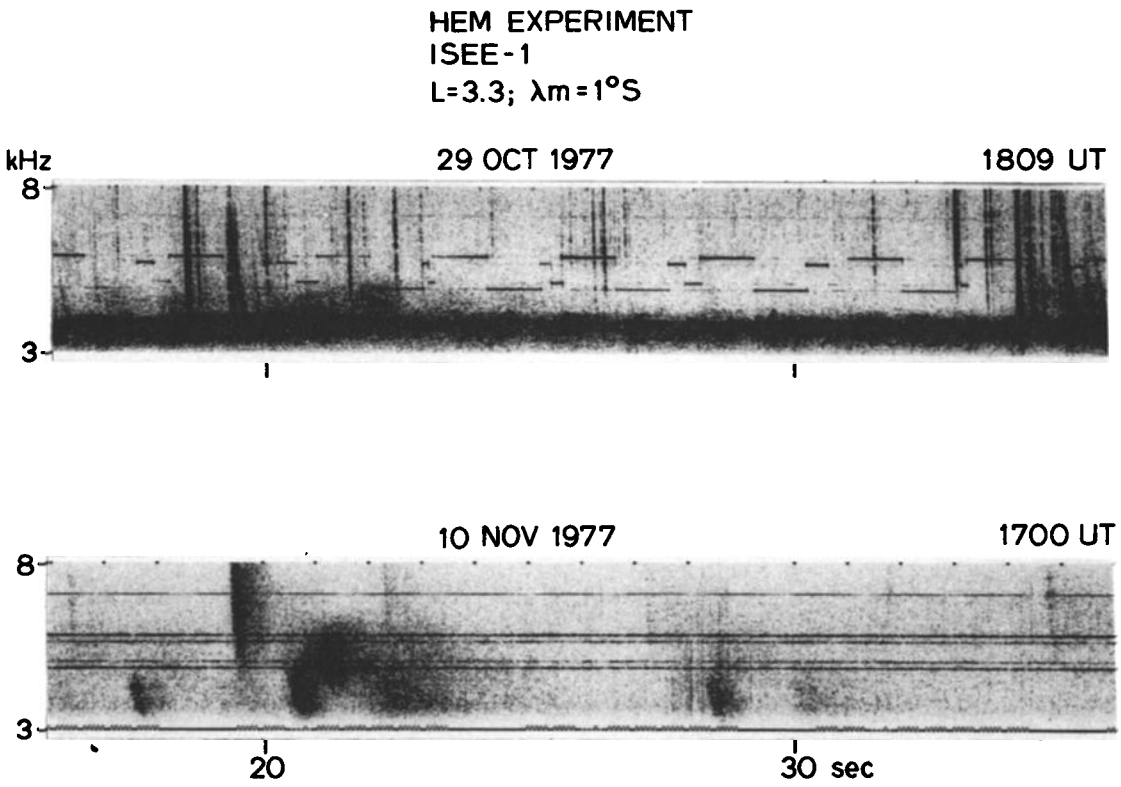

Fig. 6. VLF spectrograms of typical Siple transmitter signals observed on ISEE-1 for two of the orbits of Figure 5. The two panels show receptions on different days but at approximately the same location in space. The transmitted frequency-time format is identical in both cases. The upper panel shows well-defined pulses of standard length, indicating the existence of but a single ray path from the ground to the satellite. The lower panel shows another day with prominent multipath and/or echoing (see the appendix) effects. Note that individual pulses are virtually indistinguishable, indicating that the signals reach the satellite on various paths with group time delay differences of up to ~2 s. In the lower panel the line near 7 kHz is due to onboard interference from another experiment.

the satellite after either being magnetospherically reflected at the point where f = f_{LHR} or specularly reflected from the lower edge of the ionosphere. Some of the echoes may be reflected a number of times in both hemispheres (see Figure A1). As shown in the appendix, the direct signals would typically have a time delay of ~0.5-1.0 s, while the reflected echoes can have time delays of up to ~4 s depending on the injection latitude of the signal into the magnetosphere. In general, there would be multiple echoes associated with each direct signal, a feature in keeping with the experimental findings. In the following the terms 'direct pulse' and echoes will be employed as defined here.

Distribution of Coherent Nonducted Waves in the Magnetosphere

In this section we show that VLF signals from the Siple and North Dakota Omega transmitters are detectable continuously over large regions of the plasmasphere. In addition, we show that the intensity distribution and the group time delay of the received signals are generally smooth functions of the satellite position. As discussed in the final section of the text, the smooth variation of these parameters provides strong evidence that the observed waves have propagated to the satellite in a nonducted mode and not in a ducted mode. The widespread distribution of these nonducted waves in the magnetosphere indicates that perhaps the primary interaction between energetic particles and coherent waves from ground-based transmitters may occur in the nonducted mode.

Figure 5 shows a projection upon the magnetic equatorial plane of the ISEE-1 inbound orbits on which Siple transmitter signals were received during the period October 29, 1977, to August 2, 1978. Receptions during this period were typical of those during the 2-year period. The orbital sections along which reception occurredwere denoted by thick lines. Because of the necessity for telemetry time sharing, data could be obtained only on those orbits which fell within an operational 'window' in geographic longitude. The meridional range in which the wave injection experiment was carried out is indicated by dashed radial lines at the 50°W and the 110°W longitude positions. The receptions of North Dakota Omega signals are not indicated since those signals were observed on nearly all of the orbits shown for $1.5 < L < 4$. A typical intensity distribution of the received Omega sig-

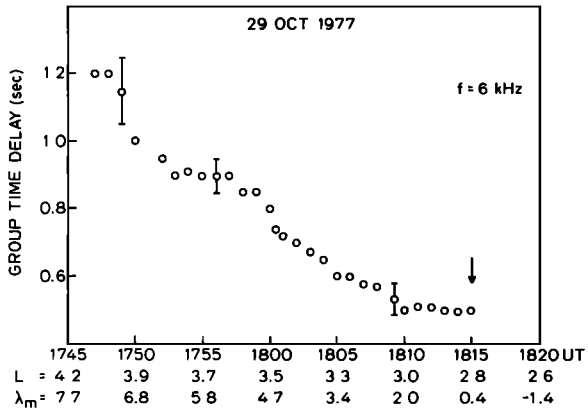

Fig. 7. Typical variation of the group time delay of Siple signals as observed on the satellite, shown for one of the orbits of Figure 5. The smooth variations of the signal time delays is an indication that the observed signals are nonducted.

nals is given in Figure 9. Our discussion of Figure 5, therefore, is limited to Siple signals. The larger probability of reception of North Dakota Omega signals as compared to Siple signals is attributable to higher radiated power (~10 kW Omega, ~1 kW Siple). In a simple dipole model the magnetic field lines through Siple and North Dakota Omega stations intersect the magnetic equatorial plane at

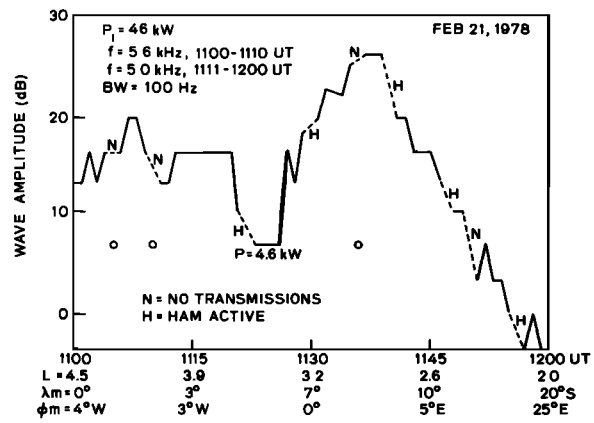

Fig. 8. The amplitude variation of the Siple signals received on ISEE-1 on February 21, 1978. The amplitude is measured in a 100-Hz band centered on the transmitter frequency. The 0-dB level corresponds to an absolute electric field intensity of ~0.1 μV/m. The southern foot of the field line passing through the satellite on this date is indicated in Figure 5. The solid lines indicate periods where the signal was received; the dashed lines indicate periods where either no transmissions were made or strong interference from another experiment (HAM) caused the receiver to saturate. The background noise level during periods of no transmissions is indicated by circles directly beneath the dashed portions. The reduction in intensity in the interval 1120-1125 UT is due to deliberate 10-dB reduction in the transmitter radiated power in this period. The L value and geomagnetic latitude λ_m are also shown.

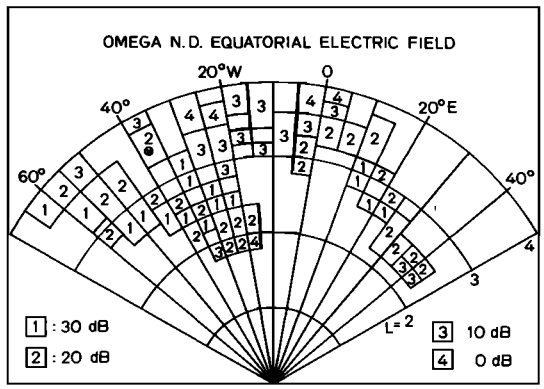

Fig. 9. The equatorial amplitude distribution of 10.2-kHz signals from the North Dakota Omega transmitter during the 9-month reference period. The amplitude in a 100-Hz band centered on 10.2 kHz is averaged within sectors measuring 5° in longitude and 0.2L in radius. In this figure, the 0-dB level corresponds to an absolute electric field intensity of ~3 μV/m. The data are based on 14 separate orbits, and there are at most two sets of points in each sector. The high intensities observed in the 0°-14° E longitude range are mainly due to a single orbit on March 29, 1978.

about L = 4.2, longitude 75°W and L = 3.5, longitude 108°W, respectively. Each intersection is marked by a circled cross.

During the period indicated, Siple signals were detected on 12 of 16 orbits during which transmissions were made. Lack of signal detection on the four other orbits was attributed to the relatively higher background noise levels that existed during the times of data acquisition. The transmitter signals were received mainly inside the plasmasphere, but reception was continuous over wide ranges of L value, magnetic latitude and longitude, and the signal time delays at the satellite varied very smoothly as a function of satellite position as illustrated in Figure 7. As discussed later in the text, these features of the data provide strong evidence that the observed signals were generally nonducted. The 'gap' in Figure 5 between L = 3 and L = 5 near the 90°W-80°W meridians is due to an absence of data for the corresponding passes for this 9-month reference period. Data from other times (e.g., October-November 1978 interval), which are not shown here, indicate that Siple signals are readily detected on the spacecraft in this region. Thus there does not appear to be any marked longitudinal variation in the probability of reception of the Siple signals.

Sample spectrograms of the Siple signals received on ISEE-1 are shown in Figure 6. The two panels show the received signal spectra for two different days for which the orbits are shown in Figure 5. Note that for both days receptions at approximately the same location in space are shown. The transmitted frequency-time format is identical in both cases. In the upper panel the individual transmitter pulses are easily distinguished since on this day there apparently was only

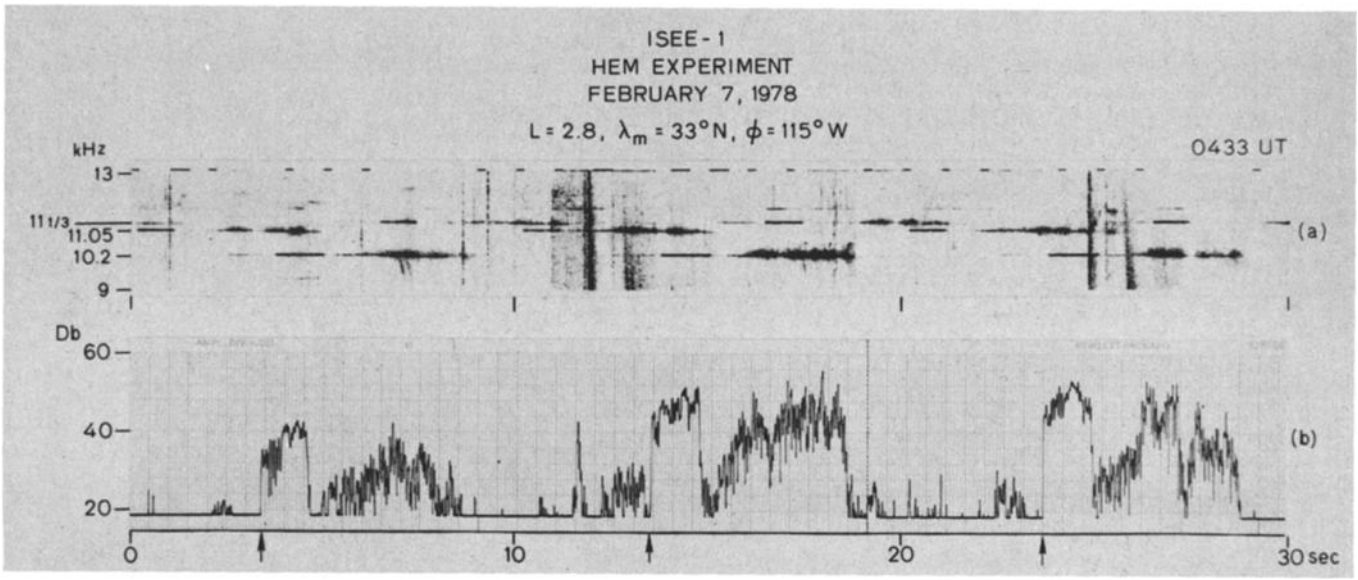

Fig. 10. North Dakota Omega signals and triggered emissions received on ISEE-1 on February 7, 1978. (a) Frequency-time spectrograms. (b) Amplitude (dB) versus time, where the arrows indicate the beginning of the reception of the direct pulse. On this day, the signal was receivedduring 0430-0440 UT as the satellite moved outward from L = 2.4 to L = 3.6, at a geomagnetic latitude $\lambda_m \simeq 33°N$. The K_p value at this time was ~2 and the satellite local time was ~2000 LT. Time code pulses appear at top of spectrogram.

one ray path available from the ground to the satellite. The reception of the same format on a day when multipath and/or echoing (see the appendix) effects were prominent is shown on the lower panel. In this case the pulses are not distinguishable, indicating that the signals reached the satellite through various paths with group time delay differences of up to ~2 s. The qualitative nature of these ray paths is similar to those shown in Figure 1 of Edgar [1976], i.e., the direct signal is associated with at least two echoes.

An interesting feature of the transmitter signals observed on ISEE-1 was the fact that the group time delay of the received signals was observed to vary smoothly as a function of satellite position, as would be expected from a distribution of nonducted rays reaching the satellite. An example of this feature is shown in Figure 7, where the group time delay is plotted versus time for the same day represented by data in the upper panel of Figure 6.

In order to prepare the plot, the group time delay of the Siple pulses was sampled once every minute. The error bars represent the measurement uncertainty associated with the plotted points, and this uncertainty decreases with time because of the increasing S/N ratio of the pulses as the satellite moves near the earth.

The plot shows that the signal time delay varied smoothly over a period of ~30 min or over a distance of ~8000 km. As discussed later in the text, the presence of ducted waves in the data would be manifested in a sharp decrease in time delay during the interval that the spacecraft was in the duct. No such decrease is evident. The lack of large variation in time delay suggests that if ducted waves are occasionally present in the data, their presence is limited to intervals of less than 1 min. Since the satellite velocity during the period of observation was approximately 5 km/s, the maximum allowable width (radial) of unobserved ducts would be approximately 300 km. Although the presence of a few of these small ducts cannot be ruled out, it is clear that they would have little overall effect on the total wave structure observed by the satellite.

The amplitude of the Siple signals as measured on the ISEE-1 spacecraft varied over a range of ~40 dB. The higher amplitudes were usually recorded on those orbits which passed close to the Siple-Roberval meridian. The data from one such orbit is displayed in Figure 8, where the 1-min average of the wave electric field amplitude is plotted as a function of time, L shell, magnetic latitude and longitude. The higher amplitudes for L > 3 correspond to times when the southern foot of the field line passing through the satellite was within 500 km of the transmitter. The type of slow amplitude change shown here as a function of L shell (shown in Figure 8) is typical of Siple signals received inside the plasmasphere on ISEE-1 and provides further support for the idea that the received signals propagate mainly in the nonducted mode.

The equatorial amplitude distribution of 10.2 kHz signals from the North Dakota Omega transmitter during the 9-month reference period is shown in Figure 9. The amplitude in a 100-Hz band centered on 10.2 kHz is averaged within sectors measuring 5° in magnetic longitude and 0.2L in radius. These data are based on 14 separate orbits, and there are at most two sets of points in each sector. Although each sector of Figure 9 is plotted in the magnetic equatorial plane, the data points used in this plot corresponds to measurements made at 5°-15° geomagnetic latitude. The equatorial intercept of the magnetic field line linking the transmitter is shown on the figure as a

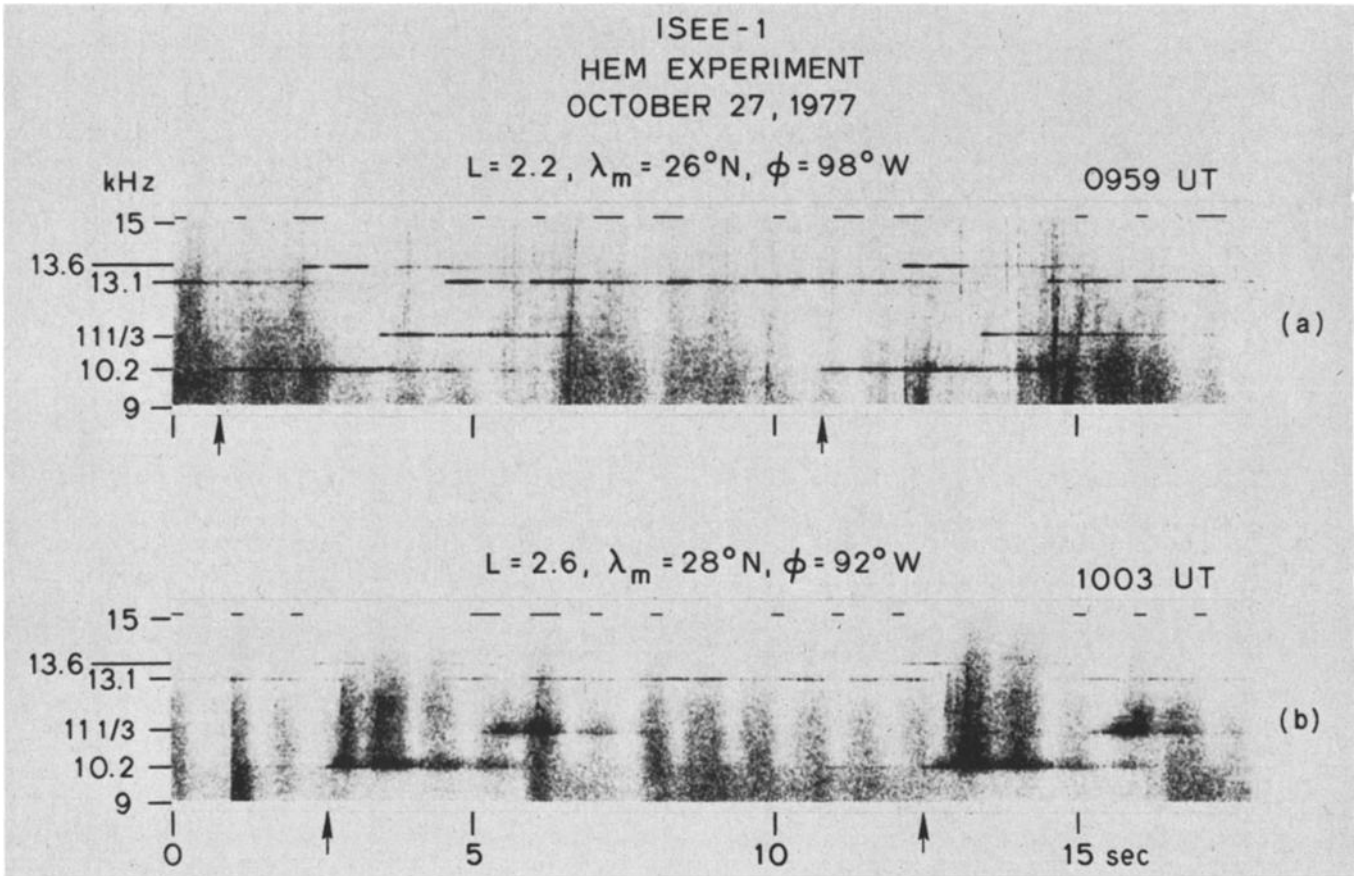

Fig. 11. North Dakota Omega signals and associated emissions received during the triggering event of October 27, 1977, as the satellite moved outward from L = 2.8 (1005 UT). The K_p value at this time was 3^+ and satellite local time was ~0400 LT. (a) Beginning of the triggering event, where arrows on the time axis indicate the instant at which the direct pulses reach the satellite. (b) Intense noise bursts triggered by the Omega signals. The intensity modulation with ~1 s period is caused by the spin of the satellite (see text). Arrows here indicate the arrival of the echo and associated emissions.

circled cross near L ~ 3.5. Note that relatively high values of wave amplitude are found not only near the field lines linking the transmitter but also on occasion at longitudes as far as 60° east of the transmitter location. The high amplitudes shown near 20°E result mainly from data obtained on a single orbit on March 29, 1978.

Since magnetic conditions at this time were disturbed, we suggest that this 'hot spot' of signal activity may have been caused by the nonlinear whistler mode instability which can amplify waves by up to 30 dB and also produce VLF emissions [Helliwell and Katsufrakis, 1974].

The absolute intensities given in Figures 8 and 9 are subject to error as much as 10 dB, due to a malfunction of the housekeeping circuitry which monitors the envelope of the received signal waveform. A joint study is presently under way with the University of Iowa experimenters on ISEE-1 [Gurnett et al., 1978] to recalibrate the Stanford experiment and refine the amplitude values given in the figures.

VLF Emission Characteristics

In this section we present examples from the ISEE-1 data set of artificially stimulated VLF emissions triggered by coherent waves from VLF transmitters. In most of the observed cases, the triggering wave appears to have been propagating in the nonducted mode when emission generation took place. Compared with triggering by ducted signals, these emissions differed principally in their spectral characteristics and in the ray path selectivity of the emission process. These differences are illustrated below with specific examples.

The first example involves signals from the North Dakota Omega transmitter at frequencies of 10.2, 11.05, and 11 1/3 kHz, as shown in the spectrogram of Figure 10a. The intensity of the Omega signal at the lower frequency, 10.2 kHz, is shown versus time in Figure 10b. Arrows along the time axis indicate the arrival time of the direct 10.2-kHz pulses at the satellite. The example shown is characteristic of the data received during a 15-min interval on this day.

The figure shows that well-defined direct pulses were received at the satellite at all three operating frequencies of the transmitter. However, only the direct pulses at 10.2, 11.05, and 11 1/3 kHz are followed by echoes with emissions (see the appendix). The direct pulses at 10.2-kHz arrive at the

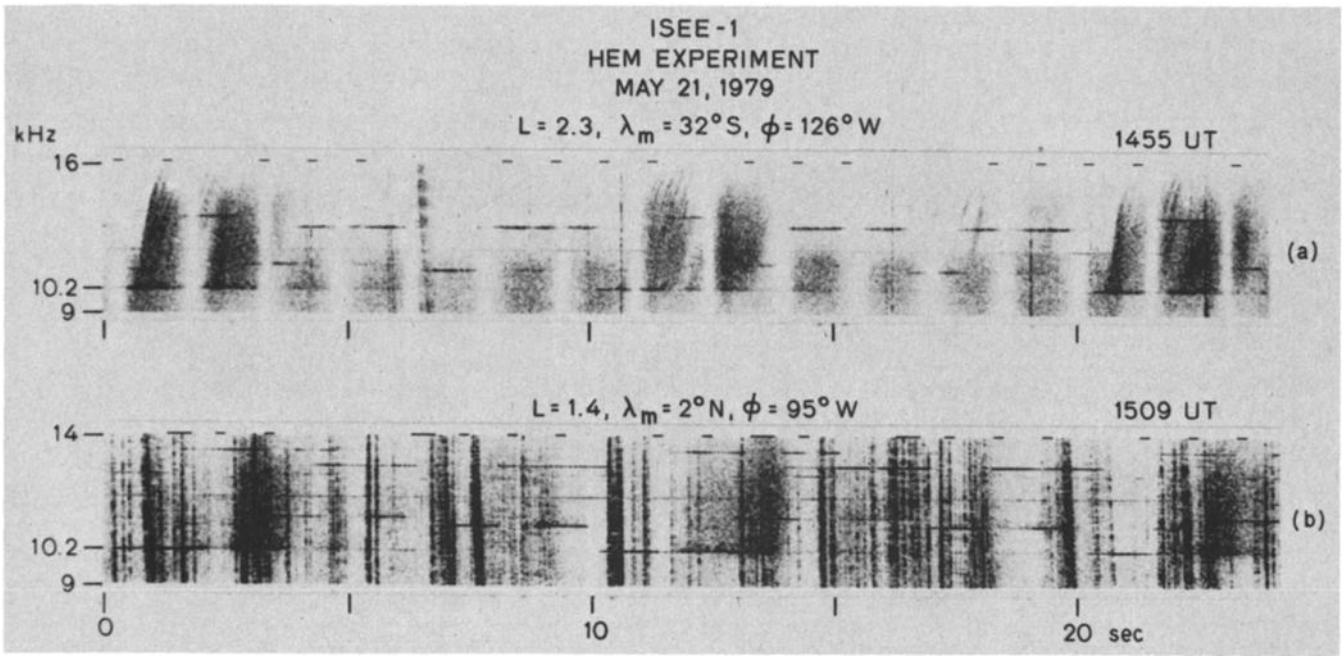

Fig. 12. Multiemission noise bursts triggered by North Dakota Omega signals on May 21, 1979, observed as the satellite moved from L = 2.3 (1455 UT) to L = 1.4 (1510 UT). The K_p value for this time period was 4^- and the satellite local time was in the range 0700–0900 LT. (a) Reception in the southern hemisphere where direct signals as well as the echoes trigger emissions. (b) Reception in the northern hemisphere where only the echo pulses trigger emissions.

spacecraft at the 3.4-, 13.4-, and 23.4-s marks, as indicated by the three arrows along the time axis. The duration of the 10.2 kHz direct pulses is approximately 1.2 s and these pulses stand out clearly in the amplitude plot in Figure 10b. Following shortly after (<0.5 s) the sharp trailing edge of the direct pulses are the echoes and associated VLF emissions.

These following signals can be identified by the fact that they exhibit much deeper amplitude fading than the direct signals. Since the duration of the direct pulses is within 50 ms of the transmitted pulse duration, we conclude that the direct rays at these frequencies reached the satellite along a single path from the transmitter. On the other hand, the associated echoes with emissions last much longer than the direct pulse. This behavior is found to be characteristic of emissions triggered by nonducted signals. The amplitude plot of Figure 10b shows that the intensity of the echo and accompanying emissions at 10.2 kHz is less than that of the direct signal. Examination of data over a 10-min period showed that the average amplitude of each emission group did

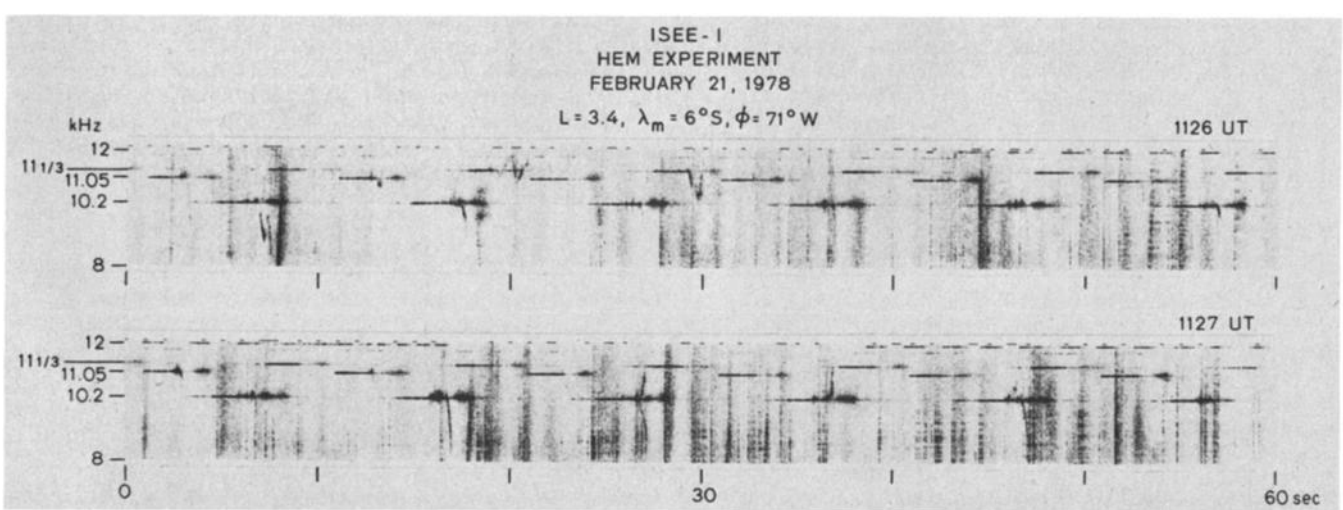

Fig. 13. Examples of the triggering event of February 21, 1978. Emissions were observed on this day between 1120–1136 UT as the satellite moved inward from L = 3.6 to L = 3.0, at a geomagnetic latitude $\lambda_m \simeq 6°S$. The K_p value for this time period was 2^+, while the satellite local time was ~0700 LT. Note that the Omega signals at three separate frequencies (10.2, 11.05, and 11 1/3 kHz) trigger emissions.

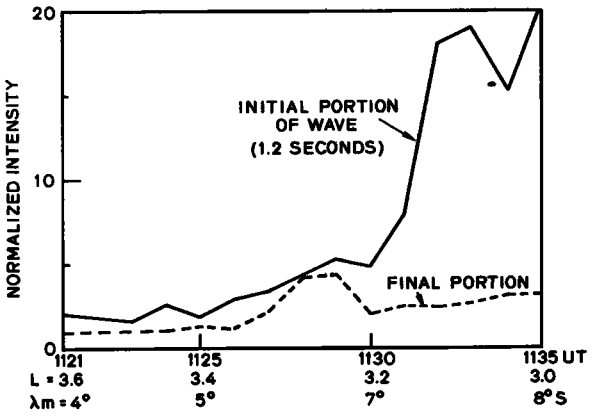

Fig. 14. The solid line shows the average relative intensity of the initial 1.2-s segment of the Omega pulses at 10.2 kHz received on February 21, 1978 (see Figure 13). The dashed line shows the average amplitude of the remaining portion of the 10.2 kHz pulses.

not appear to depend upon the average intensity of the associated direct pulse. One reason for this is that the observed direct pulses do not follow ray paths that return to the satellite as echoes. Instead, as shown in the appendix, the echoes may be produced by waves injected into the magnetosphere at magnetic latitudes higher than those of the direct pulse.

A second example of echoes with accompanying emissions is shown in the two panels of Figure 11. The data samples of the two panels are 4 min apart in time and are representatives of receptions during a period of triggering that lasted ~10 min. As in the previous example, the durations of the echo and triggered emissions are much longer than that of the direct pulse. However, the spectral characteristics of the emissions are markedly different from those of Figure 10. Figure 11a shows the wave spectrum at the beginning of the event. Arrows along the time axis indicate the instant at which the strong direct pulses at 10.2 kHz reach the satellite. The echoes and emissions arrive approximately 1 s later, producing a continuous signal of approximately 4 s duration (see the appendix). At this time the emissions consist of short rising tones of small bandwidth and relatively low intensity.

The situation is reversed a few minutes later, as shown in Figure 11b. Here the amplitude of the direct pulses at 10.2 and 11 1/3 kHz is only slightly above the noise level, whereas the echoes are strong and trigger intense multiemission noise bursts. Arrows along the time axis indicate the arrival time of the echo and associated emissions. The time delay between the direct pulse and the echo pulse is ~2 s. The emissions consist of discrete tones which rise rapidly in frequency across a 5-kHz band above the transmitter frequency. The rate of change of frequency of these rising tones approaches 40 kHz/s, a value much larger than the ~1 to 10-kHz/s rate for natural emissions observed on the ground (presumably ducted) [Allcock and Mountjoy, 1970] and natural emissions observed outside the plasmasphere [Burtis and Helliwell, 1976]. The discrete nature of the rising tones is obscured because of the large number of emissions triggered by the echo; thus they appear noiselike in character.

Spin modulation of ~1-s period is seen in the amplitude of the triggered noise bursts in Figure 11b and in the background noise near the 10-s mark. This modulation occurs at one half the spin period of the satellite (at this point in time the spin rate was 30 rpm) and results from the nonuniform excitation of the dipole antenna as it rotates in the wave field. When corrections are made for the fading due to antenna orientation, the corrected intensity of the triggered noise bursts can be shown to vary smoothly in time.

A further example of multiemission noise bursts triggered by nonducted signals is shown in Figure 12. The data shown are characteristic of receptions at the beginning and end of a ~15-min period during which triggered emissions were observed. In Figure 12a, with the satellite to the south of the magnetic equator, direct pulses at 10.2 kHz arrive at the satellite close to the 0-, 10-, and 20-s marks with the duration of each pulse stretched to ~3 s by multiple propagation paths (see the appendix). Each direct pulse group is accompanied by numerous intense emissions which arrive approximately 0.5 s after the leading

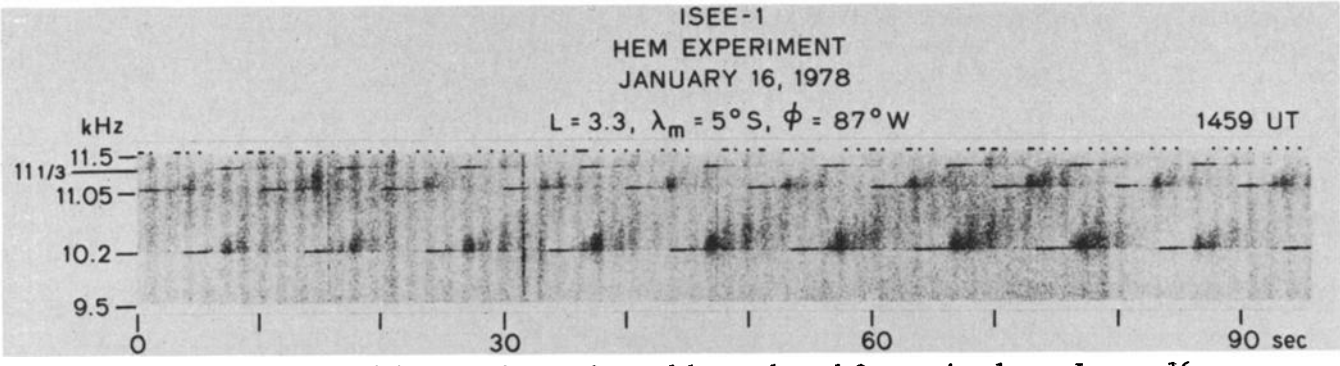

Fig. 15. The burstlike emissions triggered by nonducted Omega signals on January 16, 1978. Note the compressed time scale. Emissions were observed as the satellite moved inward from L = 3.8 (1447 UT) to L = 3.0 (1507 UT), at a geomagnetic latitude of $\lambda_m \simeq 5°S$. The K_p value was 4^- and the local time was ~0900 LT. Time code pulses appear at the top of the spectrogram.

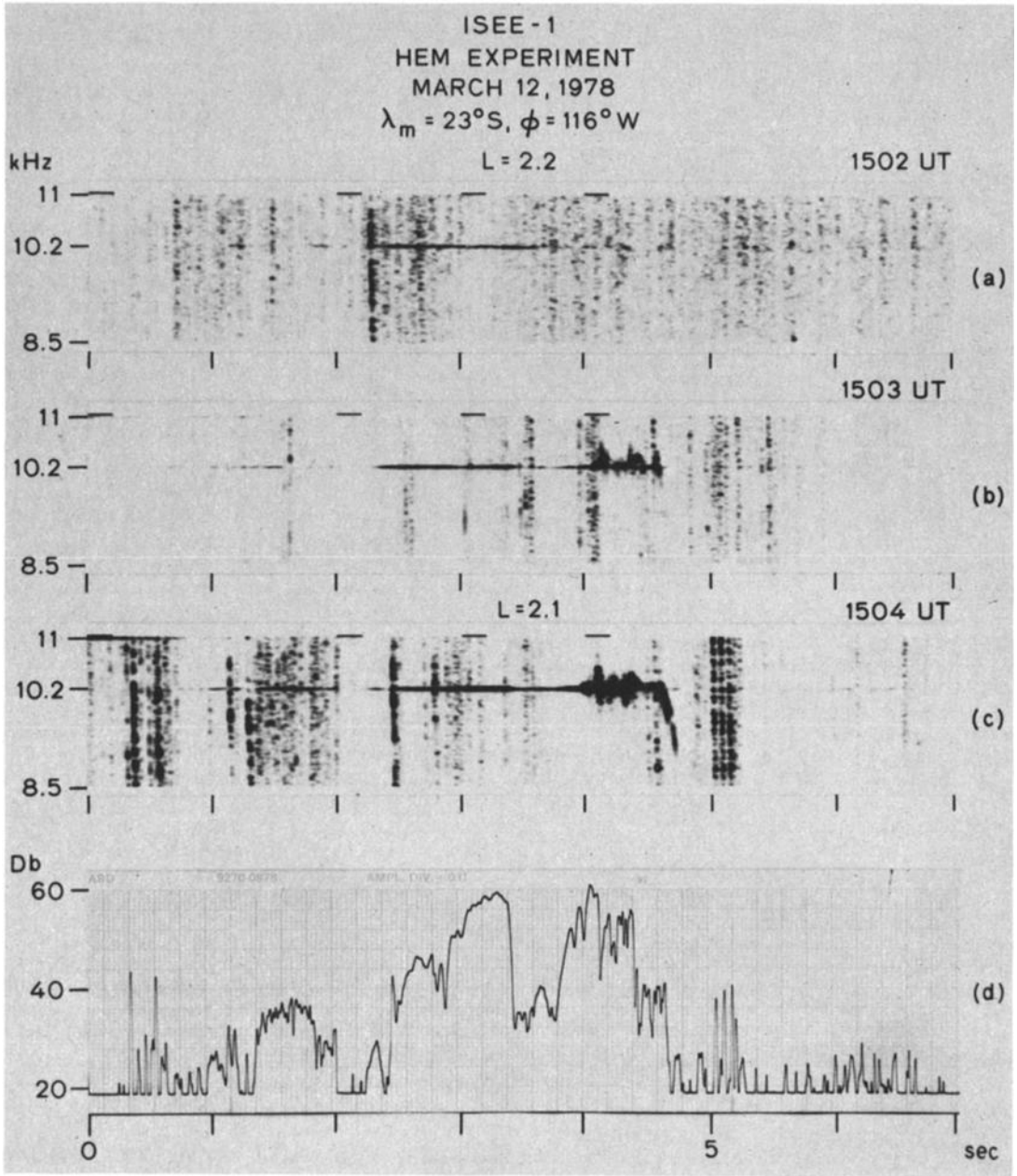

Fig. 16. The triggering event of March 12, 1978, associated with North Dakota Omega signals. The emissions were received as the satellite moved inward from L = 2.2 (1502 UT) to L = 2.0 (1507 UT). The K_p value for this time was 1^- and the local time was ~0700 LT. The North Dakota Omega signal was received shortly after the 2-s mark. The weak pulse between the 1- and 2-s marks is the 10.2-kHz signal from the Omega station in Hawaii and causes no observable triggering. (a) Beginning of triggering event; pulse duration of ~2 s indicates propagation along at least two separate paths. (b) Pulse duration of ~2.5 s indicates at least three separate propagation paths. Only pulses of longer time delay are associated with triggered emissions. (c) One of the strongest emission events. (d) Amplitude of signal shown in Figure 16 in 1-kHz band centered on 10.2 kHz.

edge of the direct pulse. Each emission group consists of hiss and discrete tones that rise ~6 kHz above the signal frequency at a maximum rate of ~30 kHz/s. These emissions resemble closely those of Figure 11 except that the latter were triggered by the echoes of Omega pulses. The frequency-selective nature of the emission process is shown by the fact that only the lowest frequency Omega pulses trigger emissions.

Figure 12b shows the wave spectrum at a later time when the satellite is in the northern magnetic hemisphere; again, the direct signals at 10.2 kHz arrive near the 0-, 10-, and 20-s marks, but now the burstlike emissions follow the leading edge of the direct pulse by approximately 1.5 s. Since no emissions are associated with the initial 1.5 s portion of the received pulses, it is clear that the shortest time delay signal does not trigger emissions.

Absence of triggering by the direct pulse of shortest time delay is found to be a consistent feature of nonducted waves. This is clearly illustrated in Figure 13. During a ~15 min period on this day all frequencies of the North Dakota Omega transmitter were received although only the lower frequencies (10.2, 11.05, and 11 1/3) were accompanied by emissions. The received signals at these frequencies consisted of a superposition of pulses which had traveled on different paths to reach the satellite. Because the duration of the pulse group at 11.05 and 11 1/3 kHz was ~2 s, at least two separate paths were available. At 10.2 kHz, the duration of the pulse groups was ~3-4 s, requiring at least three separate paths. At all three frequencies, emission generation is seen to occur ~1.5-2.0 s after the arrival of the pulse of shortest time delay, indicating that only the longer time delay pulses are involved in the triggering process.

From the spectrogram, the arrival times of the direct 10.2 kHz pulses of shortest time delay can readily be determined (near the 4.7-s mark and every 10 s thereafter). However, the arrival time of the longer time delay pulses is obscured because of pulse overlap. Pulse resolution was achieved through the use of amplitude plots similar to that of Figure 10b, making use of the fact that the amplitude and fading pattern of each overlapped pulse was generally different.

Amplitude plots (not shown) of the 10.2-kHz pulses indicated that each pulse group displayed three clearly identifiable components: (1) a direct pulse of minimum time delay with duration of 1.2 s, (2) a second pulse, also of approximately 1.2-s duration but slightly lower amplitude, which was delayed approximately 1 s with respect to the first pulse and which triggered a number of VLF emissions, including a falling tone at the pulse trailing edge, and (3) a final lower amplitude (~10 dB) pulse following shortly after the second pulse, which also was associated with VLF emissions and which was delayed 2.6 s with respect to the leading edge of the first pulse.

The apparent duration of the third pulse was more variable than the first two and lay in the range 1.2-1.6 s. Although the third pulse sometimes appeared to merge continuously with the second pulse, its separate identity was confirmed at a later stage of the triggering event when the second pulse was no longer received, while the first and 'third' preserved their characteristics.

As in Figure 10, the echoes and the associated emissions of Figure 13 are weaker than the shortest time delay pulses. This is illustrated in Figure 14 where the average intensity of the initial 1.2 s segment of the Omega pulses at 10.2 kHz is shown together with the average amplitude of the remaining portion. It is clear that the two amplitudes are not well correlated. This behavior supports the idea that the pulse of minimum time delay propagates along a magnetospheric path that differs significantly from the paths followed by a longer-delayed pulses, and that the wave-particle interactions which occur along these separate paths are signficantly different. It is surprising that the direct pulses, which do not trigger emissions, have higher amplitudes than the echoes and associated emissions since in cases of triggering by ducted waves, those signals which trigger emissions have higher amplitudes than those which do not [Helliwell et al., 1980b].

Another example of emissions triggered by nonducted waves is shown on a compressed time scale in Figure 15. The data displayed are characteristic of ISEE-1 receptions over a ~20-min period. Again, the signals at 10.2 kHz consist of a superposition of multipath pulses.

Examination of amplitude plots shows that the initial 2 s of each signal group consist of two separate overlapped pulses of 1.2-s duration, with the second pulse delayed 200 ms with respect to the first. Each double pulse group is followed after 300-500 ms by a diffuse hisslike noise burst of approximately 4-s duration, which has a sharp lower cutoff frequency of 10.2 kHz. Analogous noise bursts are triggered by the pulse groups at 11.05 and 11 1/3 kHz. Unlike previous examples of triggered emissions, these noise bursts contain no detectable structure; they are similar in spectral form to quasi-periodic noise bursts [Ho, 1974]. Since no emissions or noise are triggered during the first 2 s of the pulse group, it is reasonable to conclude that the noise is produced by longer time delay pulses which accompany, but are obscured by, the noise bursts. However, we cannot positively rule out the possibility that the unusual noise bursts were generated through some unknown delayed triggering mechanism activated by the earlier pulses.

Another type of triggered emission seen on ISEE-1, with impulsive components in its spectrum, is shown in Figure 16. Three separate events, typical of the ~5-min period during which triggering occurred, are shown. Figure 16a shows the wave spectrum at the beginning of the triggering event. The North Dakota Omega signal in all panels starts at ~2.2 s. The faint pulse between the 1-s and 2-s marks is the 10.2 kHz signal from the Omega station in Hawaii. In the discussion below we consider only the North Dakota Omega signals. Direct North Dakota pulses at 10.2 kHz arrive at the satellite along at least two separate paths, resulting in a signal duration of ~2 s. Figure 16b shows that ~1 min later, direct pulses arrive along at least three separate paths, resulting in a pulse duration of ~2.5 s and that longer time delay pulses are associated with triggered VLF emissions. Figure 16c shows one of the strongest emission events of the series. The spectral forms of the emissions in Figures 16b and 16c are discrete and impulsive in nature, suggestive of the band-limited impulses often associated with ducted waves [Helliwell, 1979].

The amplitude of the pulses and emissions of 16c is shown in Figure 16d in a 1-kHz band centered on 10.2 kHz. The pulse of minimum time delay stands out clearly; it reaches 20-dB amplitude above the pulse group immediately following and is ~1.2 s long, the nominal duration of transmitted pulses at 10.2 kHz. The

peak amplitude of the later VLF emission burst slightly exceeds that of the direct pulse. Assuming that the emissions are triggered by the later pulses, the data indicate that ~20 dB of amplification take place before the emissions are triggered. This behavior would agree well with that of emissions triggered by ducted waves [Stiles and Helliwell, 1975].

Perhaps the most important characteristic of the VLF emissions shown in this section is that the triggering was seldom seen to occur on the most direct path from the ground to the satellite. Instead, triggering took place along the paths of longer time delay.

It is important to show that this path inference characteristic is a general feature of emission triggering by nonducted waves and is not simply unique to the ISEE-1 data base or to the time frame of the ISEE mission. In this regard it can be pointed out that this path preference had previously been noted on a few occasions in data obtained on the low-altitude satellite OGO-4 during the 1967-1968 period [Angerami and Bell, 1971]. However, at the time only a few, low power (1 kW), limited duty-cycle VLF transmitters operated below 15 kHz. Consequently, the relatively few cases of emission triggering observed on OGO-4 were insufficient for establishing whether the observed path inference was an anomaly or a common feature of emission triggering by nonducted coherent waves.

Figure 17 shows an example of OGO-4 data when the satellite was close to the magnetic conjugate point of a prototype Omega transmitter at Aldra, Norway, and was observing direct signals from the transmitter at 10.2 kHz and 11 1/3 kHz. These signals were accompanied by triggered VLF emissions. The direct signals at each of the two frequencies consisted of a superposition of direct pulses that had traveled different paths to reach the satellite. The time delay of the first arriving pulses was ~0.6 s. The nonducted nature of the following pulses is evidenced in their relatively longer time delay, which is a consequence of the high wave normal angles characteristic of nonducted signals in the conjugate hemisphere [Walter and Angerami, 1969]. The nominal pulse length at both frequencies is ~1 s, while the duration of the received pulses is >2 s. Thus at least three separate paths were available to the Omega signals. Since emissions were triggered only toward the end of the pulse of longest time delay, the path selectivity of the emission triggering interactions is clearly in evidence.

Since our ISEE-1 data base contains no triggering events involving Omega signals in which the waves could be shown to be ducted, it was not possible to determine whether triggering by ducted Omega signals involves a path selectivity similar to that displayed in the case of triggering by nonducted signals. However, this important point can be investigated by examining data from other spacecraft. For instance, data from the OGO-4 spacecraft show at least three cases in which ducted Omega signals were observed to trigger VLF emissions. In none of these cases did the emission process exhibit a preference between available paths. An example from OGO-4 is shown in Figure 18. The data displayed are representative of receptions over a ~3 min period ranging from the time when the satellite entered the plasmasphere at $L \approx 4$ to the time when it reached $L \simeq 3$. Signals from the prototype Forest Port (New York) Omega transmitter at 10.2 and 11 1/3 kHz were observed during this period, and these signals were accompanied by triggered VLF emissions. The pulse duration at 10.2 kHz was ~1.5 s, somewhat longer than the transmitted pulse length of ~1.2 s. Thus the signals reached the satellite along at least two separate but closely spaced ray paths. Wave amplification and emission triggering occurred within the first 200 ms of each pulse group at 10.2 kHz, and it was evident that the pulse of minimum time delay was directly involved in the triggering process. The presence of intense falling tone emissions at the termination of each pulse group gave evidence that the pulse of maximum time delay was also involved in the triggering process. In general, the triggered

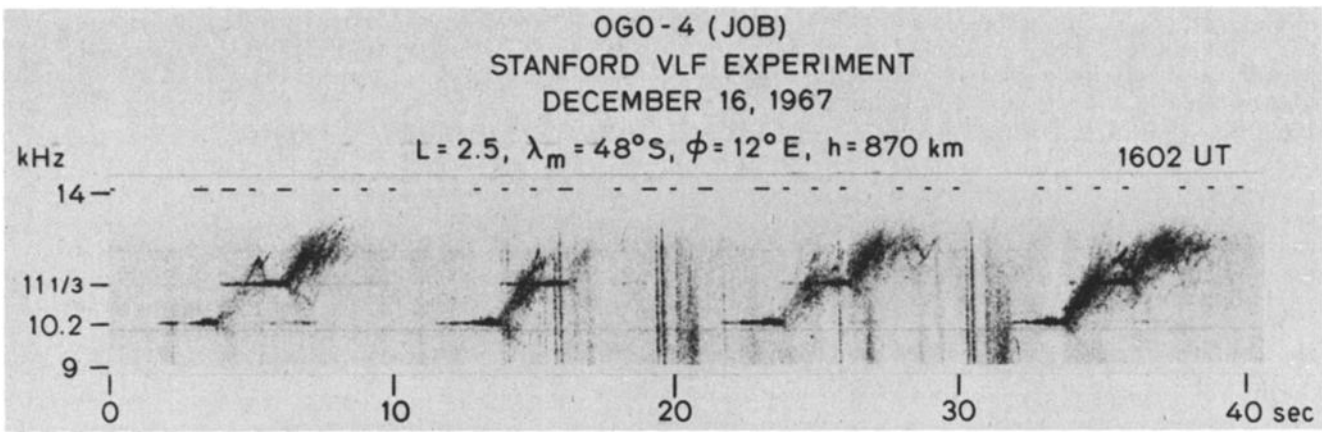

Fig. 17. Emissions triggered by signals from the prototype Omega transmitter located at Aldra, Norway, as they were received on the OGO-4 satellite on December 16, 1967. The emissions were observed during 1602-1604 UT as the polar orbiting satellite was moving southward. The K_p value at this time was 2 and the local time was ~1700 UT.

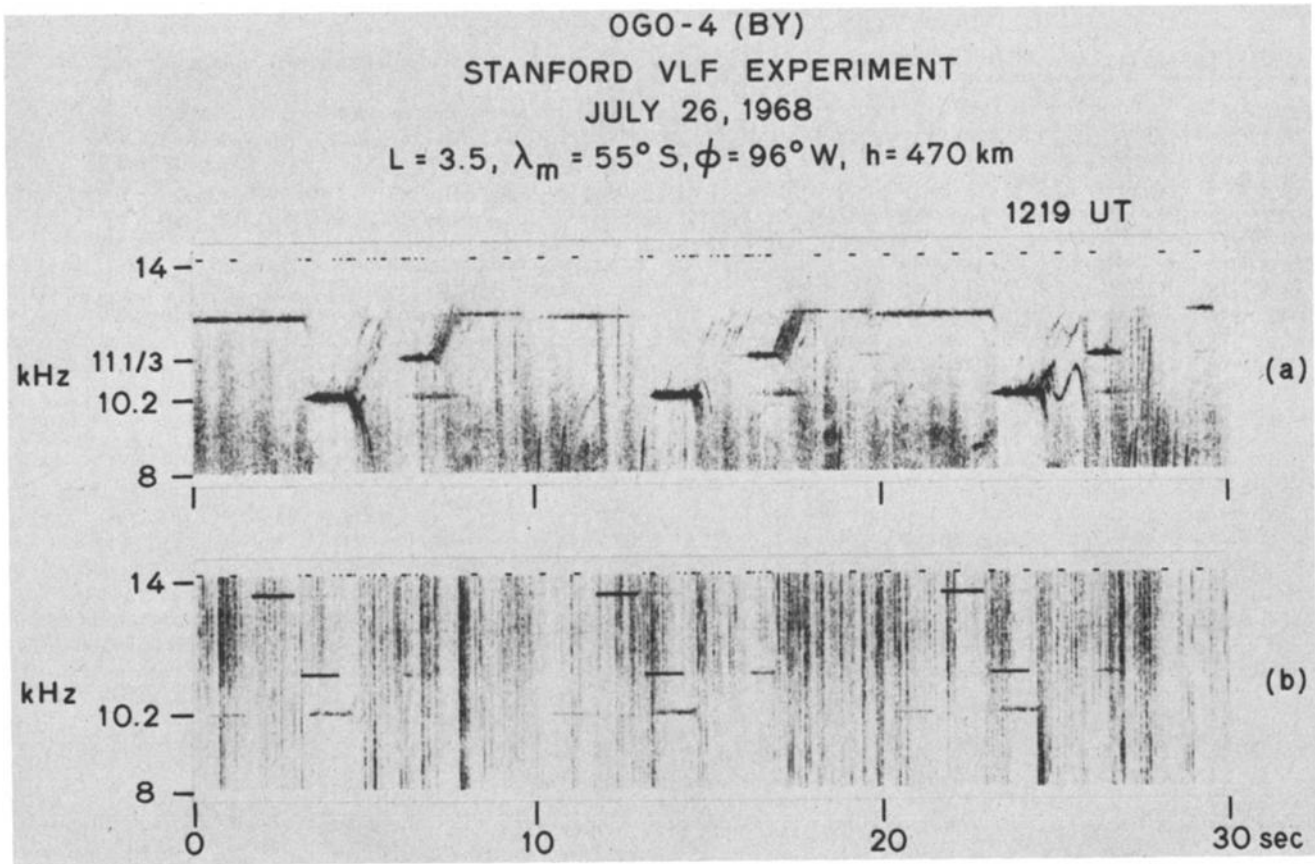

Fig. 18. (a) Emissions triggered by signals from the prototype Omega transmitter located in Forest Port, New York, and received on the OGO-4 satellite on July 26, 1968. The emissions were observed during 1217-1220 UT as the satellite was moving northward. The K_p value at this time was 3 and the local time was ~0600 LT. (b) Simultaneous VLF receptions at Byrd Station, Antarctica (119°W, 80°S).

emissions resembled closely those routinely observed at ground stations and interpreted as triggered by ducted waves.

During this event the satellite was located near the magnetic field lines linking Byrd Station in Antarctica (119°W, 80°S), and VLF data were also acquired at Byrd. A portion of this simultaneous ground data is shown in Figure 18b. The Forest Port Omega pulses at 10.2 kHz received on OGO-2 also appear on the ground records. The pulse time delay at Byrd is approximately 100 ms longer than the delay at the satellite, indicating, as expected, that the pulses received on the satellite were propagating downward. The amplitude of the 10.2-kHz pulses on the ground is rather low, and the associated emissions are difficult to detect, perhaps because of spreading losses in the earth-ionosphere waveguide.

Further evidence that the signals were ducted are the three-hop echoes of the Omega pulses at 10.2 kHz with a time delay of ~3.2 s with respect to the direct pulse. The time delay of the direct pulse is ~1.6 s, the ratio of time delays for the three-hop and one-hop pulses is 3:1, exactly as expected in a case of ducted propagation. In contrast, in cases of nonducted propagation, the ratio of time delays for three-hop and one-hop pulses is generally much larger than 3:1, since the wave normal angle increases continuously with hop number.

The Byrd data shown in Figure 18b also include ground wave signals at 10.2, 13.6, and 11 1/3 kHz from the Hawaii Omega transmitter. The ground wave signal at 13.6 kHz is strong and and evident; the signal at 11 1/3 kHz is also strong and can be distinguished by the fact that it arrives at Byrd approximately at the same time as the 10.2 kHz pulses from Forest Port Omega. The ground wave signal at 10.2 kHz is weak and difficult to see. It arrives approximately 1.2 s ahead of the ground wave pulse at 13.6 kHz. The difference in amplitude between the ground wave pulses is attributed to differential attenuation in the earth-ionosphere waveguide. These ground wave signals do not penetrate the ionosphere with sufficient amplitude to be seen in the satellite data.

Based on the OGO-4 data, there is good reason to believe that the emission triggering mechanism involving ducted coherent signals does not generally display a preference between available paths. This finding is in accord with observations from ground stations [Helliwell and Katsufrakis, 1974].

Up to this point our examples have concerned only emission-triggering events which have occurred inside the plasmasphere. In fact, only two observations of transmitter signals triggering outside (L > 4) the plasmasphere have been made with the ISEE-1 satellite, and these events have both involved signals from the Si-

ple transmitter. The apparent inability of Omega pulses to trigger emissions outside the plasmasphere can be reasonably attributed to the whistler mode gyrofrequency cutoff which, near the magnetic equator, generally confines the Omega signals to regions where $L < 4.4$.

Examples of emissions triggered by the Siple signals outside the plasmapause are shown in Figure 19; they are representative of a ~15-min period during which Siple signals were observed on ISEE-1. As shown in the figure, the transmitter pulses were occasionally observed to trigger very intense noise bursts. The upper panel shows a Siple pulse at 5.8 kHz triggering such a burst of rising emissions. The beginning of the triggering pulse is indicated by an arrow. Following this event, a second, less intense noise burst is triggered by a Siple pulse at 5.6 kHz. The lower panel shows a 1-s pulse at 5.6 kHz triggering two intense rising emissions and a weak hook-like tone which oscillates in frequency for a short time and apparently triggers a second intense noise burst consisting of multiple rising tones.

These triggering events were observed at a time when the satellite was located in the northern hemisphere on a magnetic shell outside the plasmapause at $L \simeq 9$. At such a location direct field-aligned propagation to the satellite is not possible since the equatorial gyrofrequency on this L shell is less than the transmitter frequency. However, ray-tracing studies combined with signal time delay measurements indicate that wave propagation took place in the low density region outside the plasmapause and reached the satellite after reflection from the ionosphere. The emissions triggered by the Siple pulses are unusual in that the intense burstlike structure of the emissions in Figure 19 resembles the structure of emissions triggered by ducted whistlers propagating just outside the plasmapause [Carpenter, 1978]. The triggering of this type of emission by transmitter pulses has not previously been reported. It is interesting to note that the triggering events of Figure 19 do not display a path preference characteristic such as that displayed in the Omega triggering events discussed previously.

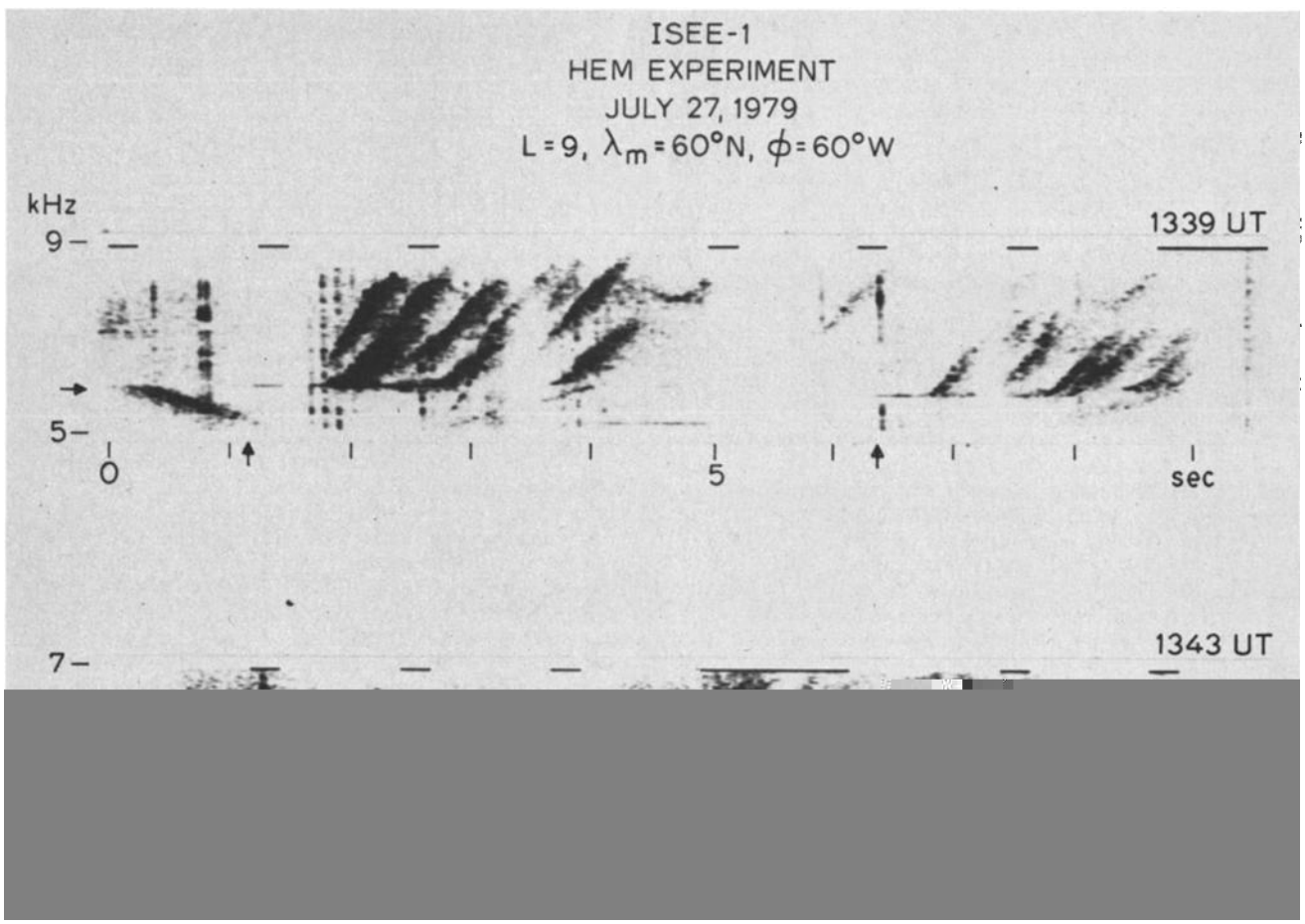

Fig. 19. Emissions triggered by Siple transmitter signals and observed on ISEE-1 on July 27, 1979. The data shown are representative of the observations during 1327-1344 UT when the satellite moved outward from $L = 6.4$ to $L = 9.6$ at $\lambda_m \simeq 60°N$. The K_p index for this time was 3 and the satellite local time was in the range ~0900-1100 LT. Note that emissions were triggered by whistlers and other natural signals as well as the Siple transmitter pulses. The locations of the transmitter pulses that are clearly triggering emissions are indicated by arrows on both the time and frequency axes.

Discussion and Conclusions

Ducted and Nonducted Propagation

In our opinion the ISEE-1 data set suggests that the bulk of the transmitter pulses observed on the satellite have not propagated to the spacecraft in a whistler-mode 'duct,' but instead have reached the spacecraft via a 'nonducted' mode.

Whistler mode ducts were originally postulated to explain the observed characteristics of multipath whistlers and whistler echo trains. Although the physical characteristics of these ducts have never been measured directly, they are generally thought to consist of field-aligned enhancements (~10%) of ionization which guide whistler mode waves somewhat as an optical fiber guides a light ray [Helliwell, 1965]. Whether these ducts are 'two-sided,' like a Gaussian perturbation, or 'one-sided,' like a step perturbation, is not clear [Gorney and Thorne, 1980; Inan and Bell, 1977]. However, indirect measurements suggest that the cross-L thickness of these ducts ranges from 200-400 km near the magnetic equatorial plane and that the radial separation of the ducts ranges from 100-1000 km [Angerami, 1970].

Long-term studies of whistler propagation characteristics at numerous ground stations suggest that the ducts are distributed throughout the plasmasphere and occupy no more than 1-10% of its volume (D. L. Carpenter, private communication, 1980).

For the purposes of the present discussion, we define a whistler mode duct to be any field-aligned structure capable of guiding whistler mode waves along a given magnetic field line with a wave normal closely parallel (<30°) to the magnetic field line direction. This is the key characteristic that a whistler mode duct must possess to explain the ground observations of whistler characteristics [Helliwell, 1965]. Thus we assume that any ducted wave will propagate closely along a particular magnetic field line with small wave normal angles.

Since nonducted waves are not guided by field-aligned structures, their propagation paths and wave normal directions will be determined by the gradients of the ambient magnetic field and background ionization. In our data the evidence for the nonducted character of the observed transmitter pulses takes three forms: (1) Continuity of the spatial distribution of the transmitter signals, (2) continuity of the amplitude distribution of the transmitter signals, and (3) continuity of the time delay distribution of the transmitter signals.

Spatial distribution. One of the outstanding characteristics of the ISEE-1 data set is the continuity of the spatial distribution of the transmitter signals. Whenever signals from a given transmitter are observed on the spacecraft near the magnetic equatorial plane, they are generally observed continuously over distances which vary from 4000-20,000 km. A widespread distribution of propagation paths is a well-known characteristic of nonducted propagation in the magnetosphere [Edgar, 1976; Walter and Angerami, 1969]. On the other hand, since whistler mode ducts were postulated in order to explain the discrete nature of multipath whistlers, they must be discretely distributed in space, and thus any array of ducted waves should be discretely distributed in space. Although it is possible that waves which have leaked from the ducts will be present in the interduct regions, these components can generally be identified through their amplitude and time delay characteristics.

Amplitude distribution. Since ducts represent guiding structures, the wave spreading loss in a duct is generally smaller than the spreading loss experienced by nonducted waves [Edgar, 1976]. Furthermore, as nonducted waves propagate within the magnetosphere, their wave normals generally swing out toward the resonance cone angle, and their refractive indices become very large compared to that of ducted waves [Walter and Angerami, 1969].

As the wave's refractive index increases, more of the wave energy is concentrated in the wave magnetic field, and the wave electric field can substantially decrease below that of a ducted wave of equal frequency and power at the same point in space. As a consequence of these two effects, it might be expected that the transmitter signals would exhibit a sharp increase in amplitude whenever the satellite entered a duct. On the basis of the study of Angerami [1970], the amplitude enhancement should endure from 1-5 min. Very few such enhancements exist in the ISEE-1 data set; instead, the transmitter wave amplitude distribution is generally smooth and continuous, as illustrated in Figure 8. This result suggests that the bulk of the transmitter signals observed on the ISEE-1 satellite have propagated to the spacecraft in a nonducted mode.

Time delay distribution. Nonducted whistler mode waves in the magnetosphere are generally characterized by large wave normal angles, large phase and group refractive indices, and relatively large travel times compared to ducted waves of the same frequency. In particular, the time delay of nonducted transmitter pulses propagating to points in the conjugate hemisphere can exceed by a factor of 2 or more the time delay of ducted transmitter pulses (of identical frequency) to the same points [Walter and Angerami, 1969]. Because of this circumstance the time delay of the transmitter pulses observed on the ISEE-1 spacecraft would be expected to show significant decreases for a period of 1-5 min whenever the satellite entered a duct. Very few such decreases have been observed in the ISEE-1 data set; instead, the transmitter pulse time delay distribution is generally smooth and continuous, as illustrated in Figure 7. Once again this result suggests that the major portion of the transmitter signals observed on the ISEE-1 satellite have propagated to the spacecraft in a nonducted mode.

In the VLF emission triggering events discussed in the previous section, the presence of the three types of evidence discussed above was assumed to be a necessary condition for the transmitter waves associated with the triggering to be labeled as nonducted waves. In addition, we required that the time delay of the various pulses in each pulse group be con-

sistent with the model of nonducted propagation given in the appendix.

Applying these same criteria to our entire data set, we conclude that the bulk of the transmitter signals propagate in the magnetosphere in nonducted modes. Furthermore, the widespread distribution of these nonducted waves in the magnetosphere suggests that the primary interactions between energetic particles and coherent signals from VLF transmitters may occur in the nonducted mode.

Frequency of Occurrence of Nonducted Wave Particle Interactions

It is instructive to compare our satellite results on nonducted waves with previous work on ducted signals observed on the ground. Carpenter and Miller [1976] showed that during the 1973-1974 time period, Siple signals were detected at Roberval on approximately 20% of the days on which signals were transmitted (72 out of 374 days). During periods of reception the average K_p was ≃2. Approximately 80% of the signals observed at Roberval were determined to have propagated along magnetic shells in the range $3.5 < L < 4.5$, and none of the observed signals was found to have propagated on magnetic shells of L values less than 3 or greater than 5.

Additional features of the Siple-Roberval correlation which did not appear in the Carpenter and Miller study are (1) the Siple signals were observed to trigger VLF emissions on 85% of the days on which signals were detected at Roberval and (2) the average K_p value during periods of emission triggering was ~2^+ in 1973 and ~2^- in 1974.

In our own study of nonducted waves we have found that for those times when ISEE-1 was within the plasmasphere at a longitude within 30° of the transmitter location, the probability of observing Siple and Omega signals was ~50% and ~80%, respectively. Thus the nonducted transmitter signals were observed on ISEE-1 much more frequently than ducted Siple signals were observed at Roberval. This result agrees well with a previous study of satellite reception of nonducted signals from the Siple transmitter [Inan et al., 1977].

There are at least two reasons for the higher probability of reception on satellites. First, ground stations such as Roberval must rely upon the presence of active whistler ducts near the station in order to guide the magnetospheric signals into the earth-ionosphere waveguide, from where they can propagate to the receiver. If ducts are not present at any particular time, the nonducted signals will suffer internal reflection in the ionosphere and will not reach the ground station. Second, the duct endpoint must lie within approximately 300 km of the receiver location or else the signals suffer too much attenuation in the earth-ionosphere waveguide and will generally not be observed [Carpenter and Miller, 1976]. The stringency of these conditions for reception of ducted signals precludes a high detection probability.

Although the probability of detecting nonducted transmitter signals on the ISEE-1 spacecraft was relatively high, the probability that these nonducted signals would trigger VLF emissions was more modest. During the period of October 1977-August 1979 the Stanford experiment on the ISEE-1 spacecraft acquired data on approximately 90 orbits within 30° of the magnetic meridian through the North Dakota Omega transmitter. Of these 90 passes, 12 containe periods in which nonducted signals from the transmitter were observed to trigger VLF emissions. Thus the probability of triggering VLF emissions by nonducted transmitter signals was ~13%. While this value is comparable to the 17% probability reported for emission-triggering by ducted Siple transmitter signals, the comparison is complicated by many factors. For instance, the radiated power of the Omega and Siple transmitters differ by 10 dB, being ~10 and ~1 kW, respectively, while the usual Siple operating frequencies are less than 6 kHz, while the Omega frequencies are greater than 10 kHz. In addition, the two transmitters are located on different magnetic shells and illuminate somewhat different portions of the magnetosphere. Furthermore, the Siple-Roberval transmissions were carried out mainly during the 0100-1000 LT interval, when emission activity is known to peak, while the satellite orbits sampled all local times equally. The importance of this latter factor is underscored by the fact that of the 12 cases in which triggered emissions were produced by nonducted waves, only two cases occurred outside the 0300-1000 LT sector. During the 12 triggering events the average K_p was ~3, a value comparable with but slightly higher than that obtained during the Siple-Roberval triggering events.

During the period of October 1977-August 1979 the probability of detecting events on the ISEE-1 spacecraft in which Siple transmitter signals triggered VLF emissions proved to be approximately 4%. This value is approximately ½ of the probability reported for ground observations of emission triggering by ducted Siple transmitter signals. One reason for the low value of this probability is the fact that due to a variety of circumstances, Siple wave injection experiments could only be carried out on 50% of the orbits in which the satellite was located in the 0100-1000 LT sector and within ±30° longitude of the transmitter. Transmissions at other local times were accomplished about 90% of the time. A second reason concerns the orbital configuration as explained above in the experiment background section.

The relatively low output power (~1 kW) of the Siple transmitter may also be an important factor, although this has clearly not been a handicap in past ground-to-ground wave injection experiments.

The Generation of VLF Emissions by Nonducted Waves

Our study has revealed important differences between the characteristics of triggered VLF emissions observed on a high-altitude satellite and those on the ground. First, the satellite emissions often consist of intense multiemission noise bursts of large bandwidth, and the maximum time rate of change of frequen-

cy of the individual emissions in these noise bursts is often as much as 3-4 times higher than that of emissions triggered by ducted waves [Allcock and Mountjoy, 1970].

Second, emissions triggered by nonducted coherent waves are regularly observed on magnetic shells as low as L = 2, while those triggered by ducted waves are not generally observed below L = 3.

Third, triggering was seldom seen to occur on the direct path of the shortest time delay from the ground to the satellite. Instead, emissions were generally triggered on longer time delay paths.

The lack of observations of emission triggering on magnetic shells below L = 3 may be due to lack of data concerning low L shells since most VLF ground stations lie at $L \gtrsim 3$, or the difference may arise because the nonducted waves interact with a different class of energetic electrons. The parallel kinetic energy necessary for nonrelativistic electron gyroresonance with 10.2-kHz waves near the magnetic equator at L = 2, assuming a cold plasma density of $N_o \simeq 4000$ cm^{-3}, is given approximately by

$$E_{\parallel} \simeq 90(\cos\theta)^{-1} \text{ keV} \qquad (1)$$

For ducted waves, $\theta \sim 0$ and the necessary parallel energy is ~90 keV. On the other hand, if the cold plasma near the L = 2 magnetic shell is in a state of diffusive equilibrium, it can be shown (see the appendix) that the wave normal angle for nonducted waves exceeds 65° near the magnetic equatorial plane, for which case, $E_{\parallel} > 200$ keV. Thus, nonducted waves should interact with higher energy, quasi-relativistic electrons, and the pitch angle distribution of these particles during disturbed times could conceivably be more favorable for the emission generation process. The fact that nonducted coherent signals can interact with inner radiation belt particles lends further credence to the suggestion that certain anomalies discovered in the pitch angle distribution of energetic electrons might be due to gyroresonance interactions in the magnetosphere with coherent VLF signals from ground transmitters [Vampola, 1978].

The sharp differences that exist between VLF emissions triggered by ducted waves and those triggered by nonducted waves may arise because of basic physical differences that exist in the generation mechanisms of these two classes of emissions.

One possibility is that nonducted signals can readily trigger emissions only at locations where the ratio of wave frequency, f, to local gyrofrequency, f_H, approaches 0.5 [Angerami and Bell, 1971]. This suggestion is based on the observation of Carpenter [1968] that ducted signals have a higher probability of triggering emissions when they propagate on field lines on which $f \approx \frac{1}{2}f_H$ at the magnetic equator. In this model the nonducted signals of shortest time delay would not be likely to trigger emissions since everywhere along their path of propagation the condition holds: $f < f_{H/2}$. On the other hand, one or more of the nonducted signals of longer time delay, which propagate on paths which reach higher L values, could reach regions where $f \sim f_{H/2}$ and could trigger emissions there. This model could be applied to a number of the cases we have shown above but does not appear to fit our data concerning emissions triggered near L ~ 2. A second possible mechanism for producing VLF emissions by nonducted waves is the longitudinal Landau resonance, the condition for which is given by

$$\omega = \bar{k} \cdot \bar{v}$$

where ω is the wave frequency, $\bar{k}$ is the wave number and $\bar{v}$ is the particle velocity. Here the waves and the particles travel in the same direction and spatial bunching of the energetic electrons is accomplished by the wave longitudinal electric field [Brice, 1964]. Since the magnitude of the longitudinal component of the wave electric field increases with the angle between the wave normal and the earth's magnetic field, it might be expected that the probability of the triggering of VLF emissions by Landau resonance also would increase with wave normal angles. For this reason, it is perhaps less likely that waves propagating along paths of shortest time delay would trigger emissions becase of their relatively small wave normal angle. Waves propagating along paths of longer time delay, however, would generally have higher wave normal angles and could perhaps more readily trigger emissions.

In order to test such mechanisms it is necessary to determine the location of the various paths of propagation and the wave normal distribution along these paths. While well-known ray tracing programs can be employed to calculate this information, the accuracy of the ray tracing depends upon the accuracy of the cold plasma density model.

At the present time we are cooperating with other ISEE-1 experimenters in an effort to map the cold plasma distribution along the satellite path on those orbits on which triggering was observed. These data will lead to more realistic cold plasma models for use in the required ray tracing study. Results of this work will be reported in the near future.

Appendix: Nonducted Wave Propagation in the Inner Magnetosphere

In this appendix we discuss typical magnetospheric VLF ray paths of 10.2-kHz signals, the North Dakota Omega transmissions shown in this paper. In calculating the ray paths we have used the Stanford VLF ray tracing program [Kimura, 1966; Walter, 1969; Burtis, 1974]. A more recent description of this program is given as an appendix by Inan and Bell [1977].

Figure A1 shows ray paths of 10.2-kHz rays injected at ~500-km altitude with vertical wave normal and at different latitudes. The point of injection is indicated by an arrow near the earth's surface. A diffusive equilibrium model is used for the cold plasma density profile [Park, 1972], while a centered dipole model is used for the static magnetic field [Mlodnosky and Helliwell, 1962]. The equatorial

cold plasma density at L = 3 is taken to be ~600 el/cm^3, whereas the plasma composition at the base level of 1000-km altitude is taken to be 70%H^+ and 30%O^+. The base level density and composition is assumed constant between 30° and 40° latitude. With this particular model the lower hybrid resonance (LHR) frequency is >10.2 kHz for altitudes near 3000 km, and the magnetospheric reflections of the 10.2 kHz rays shown in Figure A1 occur close to the point where f_{LHR} = 10.2 kHz.

In the event that the base level oxygen percentage is larger than 30% it could be the case that the wave frequency is always larger than f_{LHR}. In this circumstance the rays will not be magnetospherically reflected but instead can be specularly reflected from the lower ionosphere boundary. In the absence of horizontal gradients in the ionosphere the resulting ray paths would not be significantly different from the ones shown in Figure A1.

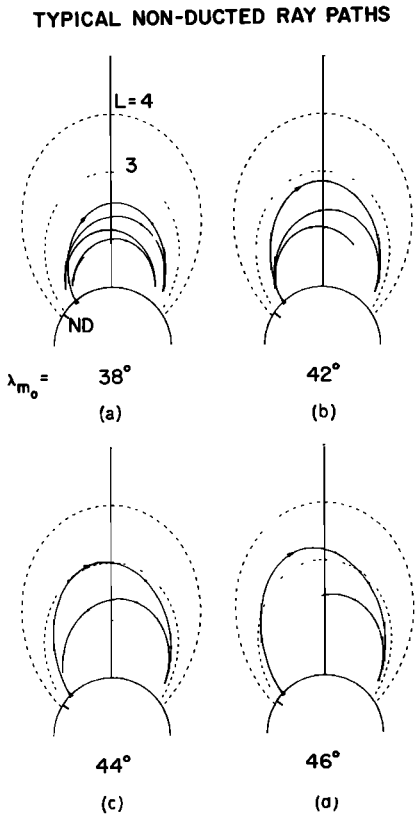

Fig. A1. Typical nonducted ray paths of 10.2-kHz signals in the inner magnetosphere. All the rays are injected at 500-km altitude with vertical wave normals at different initial geomagnetic latitudes λ_{mo}. The point of injection for each case is shown with an arrow. The dots on the ray paths are placed at 0.5-s intervals in group time delay. (a) Wave injection at 38° latitude. Signal reflects twice in each hemisphere before group time delay equals 4 s. (b) Wave injection at 42° latitude. Signal reflects once in hemisphere conjugate to source and reaches low altitude in original hemisphere before group time delay equals 4 s. (d) Wave injection at 46° latitude. Signal reflects once in hemisphere conjugate to source and reaches equator before group time delay equals 4 s.

All of the rays shown terminate at the point where the total group time delay from the initial injection point reaches 4 s. This value is representative of the largest group time delays observed on the North Dakota Omega signals. Since the rays shown are typical of rays that reach the satellite in the inner magnetosphere ($L \leq 3$), it is evident that depending on the satellite position, the transmitter signals can reach the satellite with group delays of 0.3-4.0 s. It is also clear that most points in the same region can be reached by more than one of the rays shown. When this occurs, the signal observed on the satellite is a superposition of two or more 1.2-s-long pulses with time delays that differ as much as ~3.5 s, resulting in a pulse with a duration of as much as 4-5 s on occasion. This is evidenced in the data displayed in Figures 10-12.

The initial portion of such extended pulses is due to the direct ray which arrives at the satellite prior to any reflections. Portions received with a time delay of more than 1.2 s with respect to the leading edge of the pulse are due to echoes that arrive after being magnetospherically reflected at the point where $f = f_{LHR}$ (or specularly reflected at the lower ionosphere).

As illustrated in Figure A1a, the echoes may arrive at the observations point after reflecting a number of times in both hemispheres [see also Edgar, 1976, Figure 1]. This feature is in keeping with our experimental findings.

The text discussion of Figures 10-12 employs the terminology of direct pulses and echoes with the above understanding of these terms. It should be noted that the ray path distribution shown in Figure 1A will not completely describe all of the cases shown in Figures 10-12. Some locations in the region $L \leq 3$ seem to be accessible by single ray paths only (the direct ray path); others are accessible by only two or three discrete paths not in keeping with a continuous received pulse as displayed in Figure 10. These discrepancies are due to the very simple cold plasma model that is used for computing the ray paths of Figure A1. The inclusion of horizontal gradients in the ionosphere, for instance, would affect the wave normals of injected waves at low altitudes and would cause a spreading of ray paths within a given mode. Consequently, some regions of space could be illuminated by multiple direct rays from the transmitter. Similarly, horizontal gradients in the vicinity of the reflection points would account for even further dispersion of the paths and some regions of space could be illuminated by multiple echoes of identical reflection number. Thus, for more complex models the inner magnetospheric region shown in the figure will be essentially filled with ray paths, the general character of which will be as shown. This case, the satellite could simultaneously receive pulses with group time delays of 0.5-4 s, in keeping with the ISEE-1 observations.

Typical plasmaspheric ray path distributions for lower wave frequencies typical of Siple

transmissions ($f < 6$ kHz) can be found in a study by Edgar [1976].

Acknowledgments. We deeply appreciate the valuable assistance of Dr. R. R. Anderson of the GUM experimenters group on ISEE-1 in providing data necessary to recalibrate the absolute wave amplitude data of the Stanford University receiver. We wish also to acknowledge valuable discussions with D. L. Carpenter, J. Katsufrakis, and C. G. Park concerning the ISEE-1 data. This work was supported by the National Aeronautics and Space Administration under contract NAS5-20871, and by the National Science Foundation, Division of Polar Programs, under grant DPP76-82646.

The Editor thanks S. D. Shawhan and B. Tsurutani for their assistance in evaluating this paper.

References

Allcock, G. MK., and J. C. Mountjoy, Dynamic spectral characteristics of chorus at a middle-latitude station, J. Geophys. Res., 75, 2503, 1970.

Angerami, J. J., Whistler duct properties deduced from VLF observations made with the Ogo 3 satellite near the magnetic equator, J. Geophys. Res., 75, 6115, 1970.

Angerami, J. J., and T. F. Bell, Artificially stimulated emissions triggered by non-ducted Omega transmissions, paper presented at the Commission IV, Spring Meeting, Union Radio Sci. Int., Washington, D. C., April 8-10, 1971.

Bell, T. F. and R. A. Helliwell, The Stanford University VLF wave injection experiment on the ISEE-A spacecraft, IEEE Trans. Geosci. Electron., GE-16, 248, 1978.

Brice, N. M., Fundamentals of VLF emission generation mechanisms, J. Geophys. Res., 69(21), 4515, 1964.

Burtis, W. J., Users' Cuide to the Stanford VLF Ray Tracing Program, Radioscience Laboratory, Stanford Electronics Laboratories, Stanford University, Stanford, California, 1974.

Burtis, W. J., and R. A. Helliwell, Magnetospheric chorus: Occurrence patterns and normalized frequency, Planet. Space Sci., 24, 1007, 1976.

Carpenter, D. L., Ducted whistler-mode propagation in the magnetosphere: A half-gyrofrequency upper intensity cutoff and some associated wave growth phenomena, J. Geophys. Res., 73(9), 2929, 1968.

Carpenter, D. L., Whistlers and VLF noises propagating just outside the plasmapause, J. Geophys. Res., 81, 2692, 1976.

Dowden, R. L., A. C. McKey, L. E. S. Amon, H. C. Koons, and M. H. Dazey, Linear and non-linear amplification in the magnetosphere during a 6.6-kHz transmission, J. Geophys. Res., 83, 169, 1978.

Edgar, B. C., The upper and lower frequency cutoffs of magnetospherically reflected whistlers, J. Geophys. Res., 81, 205, 1976.

Gorney, D. J., and R. M. Thorne, A comparative ray-trace study of whistler ducting processes in the earth's plasmasphere, Geophys. Res. Lett., 7, 133, 1980.

Gurnett, D. A., F. L. Scarf, R. W. Fredericks, and E. J. Smith, The ISEE-1 and ISEE-2 plasma wave investigation, Geosci. Electron., GE-16, 225, 1978.

Helliwell, R. A., Whistlers and Related Ionospheric Phenomena, Stanford University Press, Stanford, California, 1965.

Helliwell, R. A., A theory of discrete VLF emissions from the magnetosphere, J. Geophys. Res., 72, 4773, 1967.

Helliwell, R. A., Siple Station experiments on wave-particle interactions in the magnetosphere, in Wave Instabilities in Space Plasmas, edited by P. J. Palmadesso and K. Papadopoulos, p. 27, D. Reidel Publishing Company, Hingham, Mass., 1979.

Helliwell, R. A., and J. P. Katsufrakis, VLF wave injection into the magnetosphere from Siple Station, Antarctica, J. Geophys. Res., 79, 2511, 1974.

Helliwell, R. A., J. P. Katsufrakis, and M. L. Trimpi, Whistler-induced amplitude perturbation in VLF propagation, J. Geophys. Res., 78, 4679, 1973.

Helliwell, R. A., S. B. Mende, J. H. Doolittle, W. C. Armstrong, and D. L. Carpenter, Correlations between λ4278 optical emissions and VLF wave events observed at L ~ 4 in the Antarctic, J. Geophys. Res., 85, 3376, 1980a.

Helliwell, R. A., D. L. Carpenter, and T. R. Miller, Power threshold for growth of coherent VLF signals in the magnetosphere, J. Geophys. Res., 85, 3360, 1980b.

Ho, D., Quasi-periodic (QP) VLF emissions in the magnetosphere, Tech. Rep. 3464-2, Radiosci. Lab., Stanford Electron. Lab., Stanford Univ., Stanford, Calif., 1974.

Inan, U. S., and T. F. Bell, The plasmapause as a VLF wave guide, J. Geophys. Res., 82, 2819, 1977.

Inan, U. S., T. F. Bell, D. L. Carpenter, and R. R. Anderson, Explorer 45 and Imp 6 observations in the magnetosphere of injected waves from the Siple Station VLF transmitter, J. Geophys Res., 82, 1177, 1977.

Kimura, I., Effects of ions on whistler mode ray tracing, Radio Sci., 1, 269, 1966.

McPherson, D. A., H. C. Koons, M. H. Dazey, R. L. Dowden, L. E. S. Amon, and N. R. Thomson, Conjugate magnetospheric transmissions at VLF from Alaska to New Zealand, J. Geophys. Res., 79, 1555, 1974.

Mlodnosky, R. F., and R. A. Helliwell, Graphic data on the earth's main magnetic field in space, J. Geophys. Res., 67, 2207, 1962.

Park, C. G., Methods of determining electron concentrations in the magnetosphere from nose whistlers, Tech. Rep. 3454-1, Radiosci. Lab., Stanford Electron. Lab., Stanford Univ., Stanford, Calif., 1972.

Rosenberg, T. J., R. A. Helliwell, and J. P. Katsufrakis, Electron precipitation associated with discrete very low frequency emissions, J. Geophys. Res., 76, 8445, 1971.

Stiles, G. S., and R. A. Helliwell, Frequency-time behavior of artificially stimulated VLF emissions, J. Geophys. Res., 80, 608, 1975.

Vampola, A. L., Precipitation of inner zone electrons, J. Geophys. Res., 83, 2543, 1978.
Walter, F., and J. J. Angerami, Nonducted mode of VLF propagation between conjugate hemispheres: Observations on OGO's 2 and 4 of the 'walking trace' whistler and of Doppler shifts in fixed frequency transmissions, J. Geophys. Res., 74, 6352, 1969.

(Received March 12, 1980;
revised September 15, 1980;
accepted September 15, 1980.)